RSC Advances

ROYAL SOCIETY OF CHEMISTRY

www.rsc.org/advances

Research on electrochemical capacitor using transition metal hydroxides as electrode materials over the last few years has been reviewed.

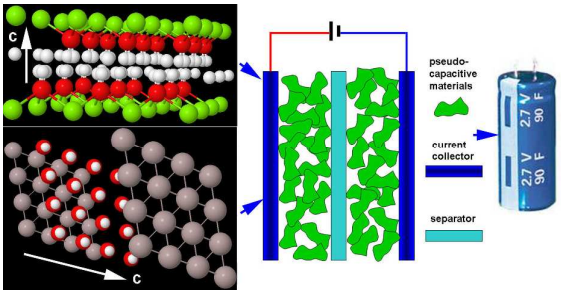

Recent development of metal hydroxides as electrode material of electrochemical capacitors

J. P. Cheng*, J. Zhang, F. Liu*

Department of Materials Science and Engineering, State Key Laboratory of Silicon Materials, Key Laboratory of Advanced Materials and Applications for Batteries of Zhejiang Province, Zhejiang University, Hangzhou 310027, P.R. China.

**Corresponding author,*
Fax/Tel.:+86-571-87951411, E-mail: chengjp@zju.edu.cn;liufu@zju.edu.cn

Abstract

Electrochemical capacitor, also called supercapacitor, is one kind of alternative energy storage devices and it has been characterized by the rapid rate of charging and discharging, and high power density. In recent years, electrochemical capacitor has attracted significant attention due to its bridging function for the power/energy gap between traditional capacitors and batteries/fuel cell. The integrated performance of electrochemical capacitor is essentially determined by the electrode materials. A review article on electrode material of electrochemical capacitors is presented, chiefly concerning transition metal hydroxides. In this work, we particularly focused on the recently published reports using cheap metal hydroxides as electrode materials of electrochemical capacitor, based on the classification of metal hydroxide by composition and microstructure. Some important experimental data on this issue are indicated and summarized. Furthermore, a brief discussion on future development, challenges and opportunities in this area is also provided.

1. Introduction

Energy storage is very critical for efficient, clean and versatile use of energy and is also a key element in harvesting energy for renewable energy. Batteries can keep our electronic devices working for a long time due to their high energy densities. For rapid power delivery and recharging, electrochemical capacitors (ECs) are suitably used. Electrochemical capacitors, also called supercapacitors, which can operate at a high charge/discharge rate over a large number of cycles, are one kind of important devices for energy storage.[1] ECs can store electrochemical energy by either ion adsorption as electrochemical double layer capacitor (EDLC) or fast surface red-ox reactions like batteries.[2] The performance of ECs is essentially determined by the electrode materials. The most widely known electrode materials for red-ox actions of ECs are RuO_2 and MnO_2. Recently, this list has been expanded to other metal oxides, as well as hydroxide, nitrides, and carbides. Thus, a lot of transition metal oxides and hydroxides like MnO_2, Fe_3O_4, $NiCo_2O_4$, V_2O_5, $Ni(OH)_2$, and $Co(OH)_2$ have been extensively studied as the electrode materials of supercapacitors, enabling fast reversible red-ox reactions on their surfaces.[3] Regarding the charge storage mechanism of ECs, EDLCs and pseudocapacitors can be generally determined. Although EDLCs based on carbon electrode materials have a good stability, their charge mechanism limits the specific capacitances in a range of low values. Thus, ECs based on pseudocapacitor usually can exhibit a much higher specific capacitance than EDLCs. Among the candidate electrode materials for pseudocapacitor, oxides and hydroxides of transition metals present high specific capacitance due to their rich red-ox properties involving multiple oxidation states.

Recent years there have yielded great progress in the theoretical and practical research and development of ECs, as evinced by a large number of research papers published. Low-cost and environmentally friendly ECs with the capability of storing large amount of electrical energy have potential applications in electric vehicles, energy storage for renewable energy production, portable electronics and large industry equipments. Thus, an elegant way of achieving high energy density is to design hybrid systems by using earth abundant metal oxides or hydroxides as the electrode materials of ECs. Because there have many review literatures related on the advances of metal oxides electrode materials for ECs,[4-13] we will focus on the development of metal hydroxide such as cobalt- and nickel hydroxides in this paper.

In this review, we survey the recent reports of earth abundant metal hydroxides as electrode materials of ECs, typically from 2009 to now. With an attempt to review transition metal hydroxide materials for ECs, we discuss the preparation and modification of them. This will be followed by the classification of metal hydroxide by composition and microstructure. They are grouped into several sections including single-, binary metal hydroxides, hydrotalcite-like compounds, hierarchical hybrids of metal hydroxide and metal oxide, and asymmetric supercapacitors based on metal hydroxide. Finally, we will discuss the potential directions that might be expected to take for ECs research. We believe that the topic of this review is interesting to the scientists working in the related fields.

2. Single Co- or Ni- hydroxide

2.1 Single crystalline hydroxide

Single crystalline metal hydroxide as an electrode material of ECs has been commonly reported and investigated in many published papers, typically for these transition metal hydroxides containing the elements including nickel, cobalt and iron. These metal hydroxides are

often layered materials with a large interlay spacing and they can have very high theoretical specific capacitance. Then, we will firstly focus on these interesting results reported using single metal (Co- and Ni-) hydroxide as electrode materials of ECs in this section.

2.1.1 β-cobalt hydroxide

Cobalt hydroxides have been attractive as the electrode materials of ECs due to its layered structure with a large interlayer spacing (0.46 nm), their well-defined electrochemical red-ox activity, and the possibility of enhanced performances through different preparation methods. Their sheet or plate-like shapes are beneficial in improving the electrochemical performance, providing a large inter-sheet spacing for ions transferring and high utilization of electrode materials. Uniform β-$Co(OH)_2$ crystals reported as electrode material of ECs could be easily prepared by chemical, [14-20] hydrothermal methods,[21] electrodeposition. [22] Usually, these $Co(OH)_2$ platelets have a hexagonal morphology lying on the (001) planes.[18] The $Co(OH)_2$ nanoplates prepared by Mustafa *et al.* exhibited a high specific capacitance of 1012.7 F/g and good capacity retention of ca. 92% after 1,000 continuous charge–discharge cycles.[14] Ji *et al.* prepared cobalt hydroxide thin film supercapacitor *via* screen printing onto a plastic substrate to make a flexible model, as shown in **Fig. 1**. [20]

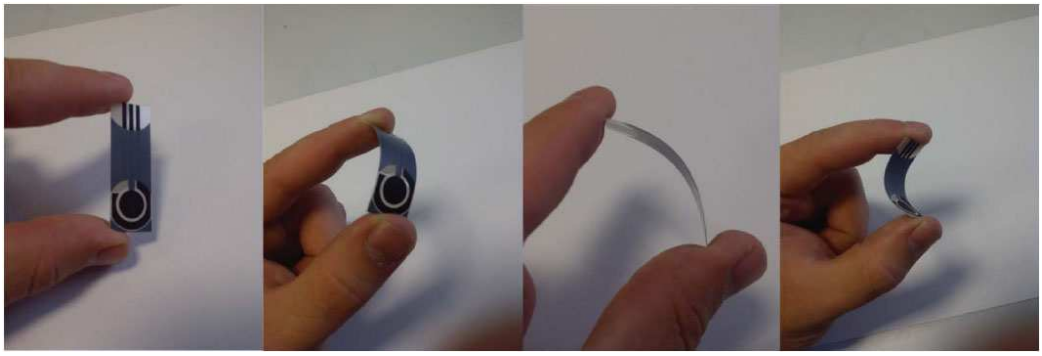

Fig. 1 Pictures depicting a flexible graphite screen printed electrode. Taken from Ref. 20 with permission from RSC Publications,

Since we all know that the supercapacitive performance of electrode materials strongly depends on their morphological creation and thereby on the specific surface area. Thus, porous three dimensional (3D), hierarchical structures of $Co(OH)_2$ such as coral-like,[23-24] flowerlike shapes,[20,25-31] mesoporous nanowires,[32-35] nanoflake films,[36-42] nanocone arrays,[43] and hollow core-shell structures were fabricated and developed for ECs applications. The surfaces of these 3D $Co(OH)_2$ structures show randomly distributed, interconnecting configurations, resulting in a network-like structure with many cavities between the adjacent blocks. The high specific surface area and numerous pores in the 3D $Co(OH)_2$ can facilitate the penetration by electrolytes and thus contributed to the excellent capacitive properties. Thus, a lot of relevant methods have been developed including electrodeposition, hydrothermal method, liquid-precipitation, ionothermal synthesis[44], ball-milling [19] and sonochemical synthesis.[15]

Ionic liquids (ILs, 1-butyl-3-methylimidazolium tetrafluoroborate) and $Co(OH)_2$ could form a nanohybrid with a large surface area of 400.4 $m^2 g^{-1}$ by ionothermal synthesis, as shown in **Fig. 2**. The IL-$Co(OH)_2$ based electrode exhibited a higher specific capacitance of 859 F g^{-1} with a high-rate capability, better cycling performance, higher ion diffusion coefficient and lower charge

transfer resistance than bare $Co(OH)_2$.[44] Theoretical calculations revealed that IL molecules consisting of anion and cation groups enabled easier hydrogen desorption/adsorption process, leading to a favorable red-ox reaction on the $Co(OH)_2$ surface.

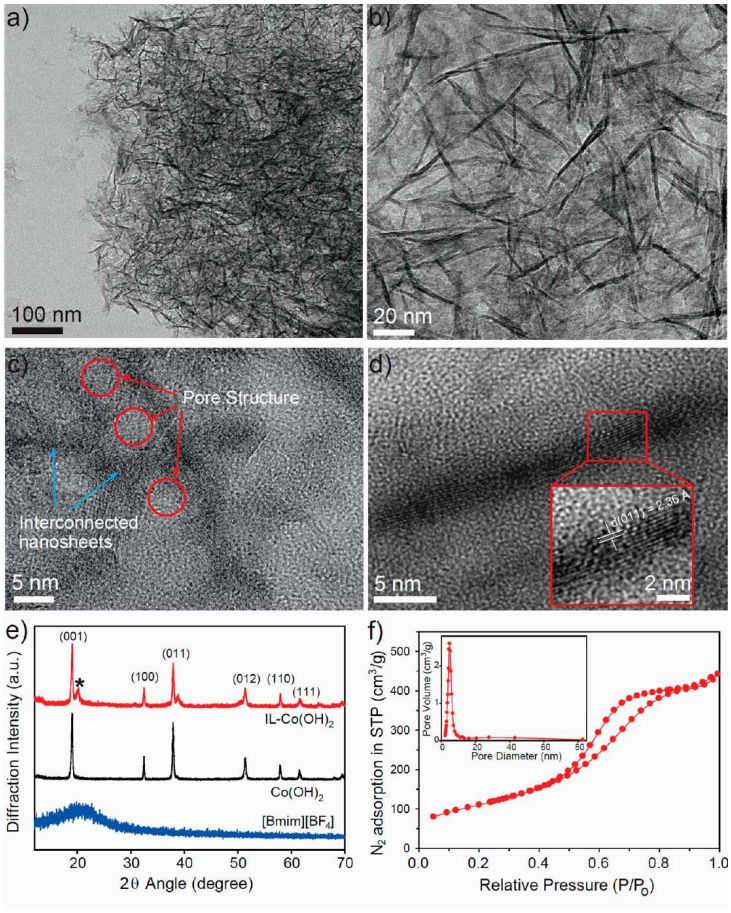

Fig. 2 (a-d) TEM image of IL-$Co(OH)_2$ (inset of image d shows a lattice image of individual IL-$Co(OH)_2$); (e) XRD patters of IL-$Co(OH)_2$, $Co(OH)_2$, and [Bmim][BF_4]; (f) Nitrogen adsorption/desorption isotherms and pore size distribution of IL-$Co(OH)_2$. Reprinted with permission from Ref. 44. Copyright (2013) American Chemical Society.

If $Co(OH)_2$ films can be directly deposited on a current collector, the $Co(OH)_2$ electrodes will have several advantages including without using polymer binder and conducting agent. Therefore, preparation of $Co(OH)_2$ films is an other excellent route to obtain high-performance electrode materials.[45] Among various synthetic methods, electrodeposition is rather popularly used. Li *et al.* compared various electrochemical tests of ordered mesoporous $Co(OH)_2$ films on foamed nickel and titanium plate.[39] The $Co(OH)_2$ film on foamed Ni foam had a much higher specific capacitance (maximum: 2646 F g^{-1}) than that on titanium plate (maximum 1018 F g^{-1}) due to the larger surface area of Ni substrate. More recently, Salunkhe *et al.* have applied chemical deposition method to synthesize $Co(OH)_2$ rods films on the current collector.[46] The direct growth of $Co(OH)_2$ rods gave an open-three dimensional structure for easy access of electrolyte throughout the material surface, being an efficient electrode for ECs application. The electrode achieved the highest capacitance of 1116 F g^{-1} at a current density of 2 A g^{-1}.

It is known that β-form $Co(OH)_2$ possesses a brucite-like origin, where octahedral with divalent cobalt cations six-fold coordinated by hydroxyl ions share edges to produce 2D charge-neutral layers stacked one over the other without any anion. Most as-fabricated β-$Co(OH)_2$ crystals have a lot of crystalline planes parallel stacking along the [001] direction. However, single layer β-$Co(OH)_2$ nanosheets could be prepared by phase transformation from exfoliating layered α-$Co(OH)_2$ in formamide at 80 °C under nitrogen gas protection for 15 hours.[47] The obtained β-$Co(OH)_2$ nanosheets were measured with lateral size from several tens to several hundred nanometers and thickness in the range of 0.9 to 1.3 nm. The selected area electron diffraction (SAED) image taken from an individual nanosheet corresponded to the crystalline structure of β-$Co(OH)_2$, as shown in **Fig. 3**. The as-prepared single-layer β-$Co(OH)_2$ nanosheets could be assembled with graphene oxide (GO) to form a two-dimensional composite. The reduced GO/β-$Co(OH)_2$ composite exhibited a high specific capacitance up to 2080 F g^{-1} at the current density of 1 A g^{-1}.

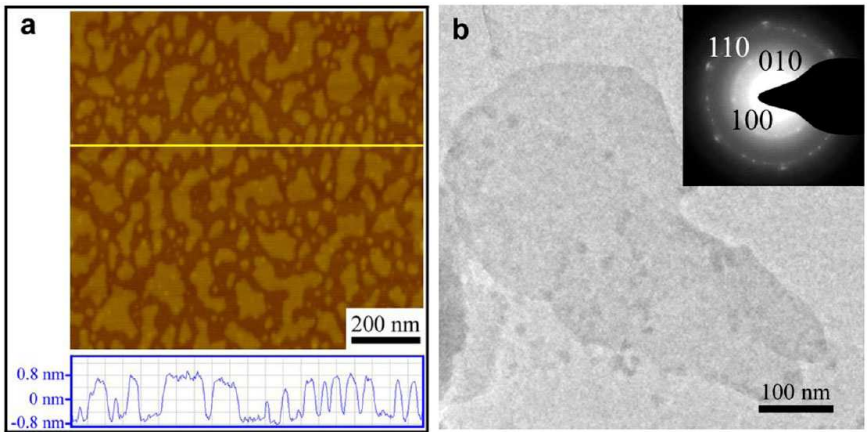

Fig. 3 (a) AFM and height profile, (b) TEM and SAED images of single-layer β-$Co(OH)_2$ nanosheets. Reprinted with permission from Ref. 47. Copyright (2014) American Chemical Society

Traditionally, the theoretical specific capacitance of inorganic pseudocapacitors can be calculated according to the transferred electric charge and weight of active electrode materials. The theoretical specific capacitance of active material can be calculated as $C_t = (n \times F)/(M \times \Delta V)$, where n is the moles of charge transferred per mole of active material, F is Faraday's constant, M is the molar mass of the electroactive phase, and ΔV is the operating voltage range.[17a] The theoretical value C_t of $Co(OH)_2$ is 3460 F g^{-1} (within 0.6 V), assuming that all $Co(OH)_2$ phase in the bulk is electrochemically accessible and contributes to the redox reactions.[17a] However, most reported experimental values are still lower than the theoretical values. The difficulty in approaching the theoretical specific capacitance is strongly associated with the limited ion diffusion within conventional dense electrode film and poor electron transfer due to the semiconducting or insulating property of the cobalt compounds, which make them not fully take part in the electrochemical reactions. Thus, much effort still needs to done in order to improve the electrochemical performance of $Co(OH)_2$.

2.1.2 Nickel hydroxide

Nickel hydroxide has been widely used as an electrode material in commercial alkaline rechargeable batteries. Recent reports have proved that it is also an outstanding candidate for

pseudocapacitors owing to its well-defined electrochemical red-ox activity, high specific capacitance, low cost, improved environmental compatibility, and various crystalline morphologies. Thus, $Ni(OH)_2$ is deemed as an active transition metal hydroxide material for ECs, too.

To obtain a high specific capacitance and good rate capability, nanoscaled $Ni(OH)_2$ crystals were thus prepared owing to its high surface area and abundant pores. $Ni(OH)_2$ nanosheets with high surface area and narrow pore size distribution could be facilely synthesized by microwave assisted heating method and applied as electrochemical pseudo-capacitive materials for ECs,[48] exhibiting a high specific capacitance of 2570 F g^{-1} at the current density of 5 A g^{-1} with a good cycling stability. Shao *et al.* reported that rare metal La-doped nano nickel hydroxide was prepared by electrodeposition and it could reach the highest discharge capability of 840 F g^{-1}.[49]

It is well accept that porous structures can accelerate the diffusion of active species and facilitate electron transportation. 3D Loose-packed porous $Ni(OH)_2$ used as electrode materials was commonly prepared by various method, including different morphologies such as coral-like[50] microsphere of nanoflakes,[51] snow-ball like,[52-53] coin-like plates,[54] flowery architecture,[55-56] pompon-like,[57] nanotube arrays,[58] hollow microspheres,[59] nanowire aggregations[60] *etc*. These porous structured $Ni(OH)_2$ with low densities and high surface areas have thus attracted much attention not only for their importance in achieving a better understanding of the formation process but also due to their numerous potential technical applications such as ECs.

To date, many attempts have been made on the synthesis of 3D nano- and micro-structured hollow $Ni(OH)_2$. Some metal oxide nanoarrays (such as ZnO) could be used as a template to fabricate hollow $Ni(OH)_2$ nanotube electrode material, as shown in **Fig. 4**. The opening of the $Ni(OH)_2$ nanotube arrays provides many channels that facilitate the penetration of the electrolyte and ions deep into the electrode, leading to an increase in surface area for electrochemical reaction.[58,61]

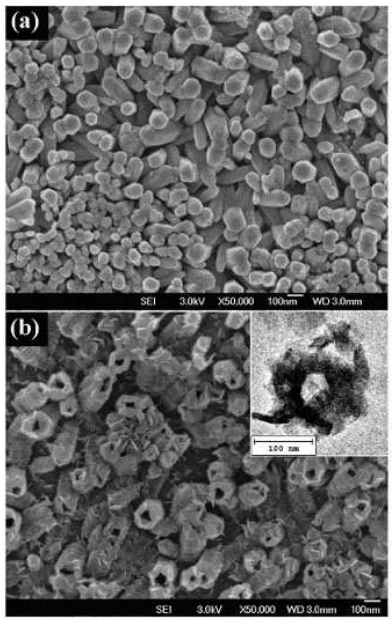

Fig. 4 SEM micrographs of (a) ZnO nanorod arrays and (b) nickel hydroxide nanotube arrays after etching with 6 M NaOH. Inset in b is a top-view TEM micrograph of the nickel hydroxide nanotube. Taken from Ref. 58 with permission from RSC Publications.

Because 3D mesoporous nanostructure films can enhance the supercapacitive performance by reducing the diffusion resistance of electrolytes and enhancing the ion and electron transportation,[62] ultrathin $Ni(OH)_2$ nanowall films deposited on Ni foam with an ultrahigh capacitance of 2675 F g^{-1} and up 96 % reversibility was reported by Sun *et al.*,[63] as shown in **Fig. 5**. This specific capacitance is beyond the theoretical value of β-$Ni(OH)_2$ (2358 F g^{-1} within 0.44 V), perhaps it is attributed to the combination of the Faradic capacitance from chemical reactions and the EDLC from the high surface area. A much higher specific capacitance observed on a $Ni(OH)_2$-nickel foam composite was 3152 F g^{-1} at a current density of 4 A g^{-1},[64] where loosely packed nanometer scale $Ni(OH)_2$ grains spread on nickel foam maintained a greater surface area for reaction and resulted in the effective utilization of electrode material. Both α-$Ni(OH)_2$ and β-$Ni(OH)_2$ films could be electrodeposited directly on nickel form at different temperature. The sample synthesized at 65 °C possessed a porous honeycomb-like structure and the highest specific capacitance was up to 3357 F g^{-1} at a current density of 4 A g^{-1}.[65] Above reports reveal the possibility to exceed the theoretical Faradic capacitance of $Ni(OH)_2$. These $Ni(OH)_2$ crystal films usually have a 3D porous structure, ultrathin morphologies and direct-connection to conductive substrates. In addition to electrodeposition,[66-69] other methods such as chemical bath deposition,[70-72] hydrothermal method [73-78] were also reported to controllably fabricate thin $Ni(OH)_2$ films and they were applied as the electrode materials of ECs with a high specific capacitance.

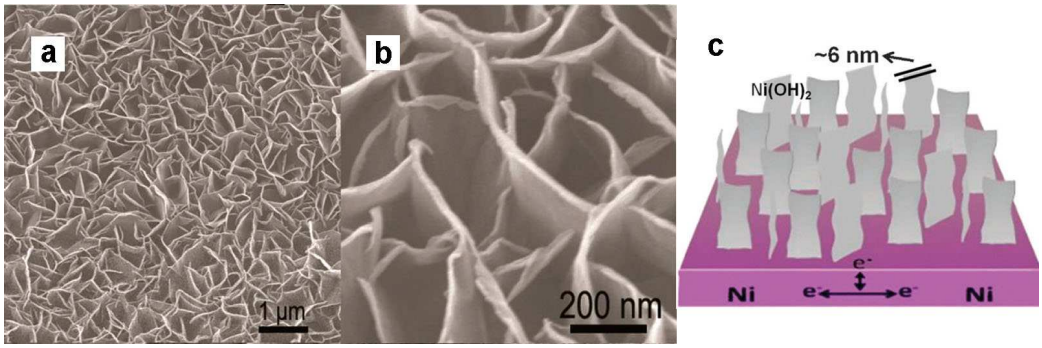

Fig. 5 (a,b) Low- and high- magnification SEM of $Ni(OH)_2$ nanowall films; (c) schematic image of the $Ni(OH)_2$ nanowall films. Adapted from Ref. 63 after modification with permission from RSC Publications.

Lokhande *et al.* found that $Ni(OH)_2$ thin films with different nanostructures such as nanoplates, stacked nanoplates, nanobelts and nanoribbons could be controllably fabricated by varying the deposition temperature.[78] These electroactive $Ni(OH)_2$ films grown on conductive substrates can be directly used as a binder-free electrodes and such electrode design has two advantages over conventional thin film electrodes: (1) the poorly intrinsic conductivity of the electroactive material is no longer a big concern due to the directly attachment of electroactive materials to the conductive substrate; (2) this design make other auxiliary components like conductive agents and binders completely unnecessary. Thus, $Ni(OH)_2$ films *in situ* deposited on a conductive substrate are of great potential for ECs application.

Though $Ni(OH)_2$ has a lower theoretical specific capacitance than $Co(OH)_2$, the reported specific capacitance values of $Ni(OH)_2$ are usually much higher, compared with $Co(OH)_2$. We assume that the formed structure and morphology of $Ni(OH)_2$ are more suitable for

electrochemical reaction than those of $Co(OH)_2$. Considering that Ni is much cheaper than Co, $Ni(OH)_2$ is thus a promising electrode material for ECs.

2.2 Amorphous monometallic hydroxide

Because a metal hydroxide with poor crystallinity or amorphous phase may result in more transportation channels than that of a highly crystalline one, some reports on the fabrication and electrochemical properties of amorphous metal hydroxides are published. Tong and co-workers carried out some research on the amorphous nickel- and cobalt hydroxides.[79a] They applied electrochemical method to prepare amorphous nickel hydroxide nanospheres (as shown in **Fig. 6**), exhibiting a high specific capacitance (2188 F g^{-1}). The asymmetric pseudocapacitors made of the amorphous nickel hydroxide had a high capacitance (153 F g^{-1}), a high energy density (35.7 Wh kg^{-1} at a power density of 490 W kg^{-1}) and super-long cycle life (97% and 81% charge retentions after 5,000 and 10,000 cycles, respectively).[79a] Cao group synthesized amorphous mesoporous $Ni(OH)_2$ nanoboxes with uniform size of 450-500 nm by template-engaged route. [79b] The mesoporous $Ni(OH)_2$ hollow nanoboxes showed high specific capacitance of 2495, 2378, 2197, 1993 F g^{-1} at discharge current of 1, 2, 5 and 10 A g^{-1}, respectively.

Amorphous $Co(OH)_2$ nanostructures with excellent electrochemical behaviors could be synthesized on graphite flakes by a simple and green electrochemical method in deionzied water without using any chemical additives. These amorphous cobalt hydroxides having three-dimensional structure possessed a high specific capacitance to 1094 F g^{-1} at a scan rate of 1 mV s^{-1}, its specific capacitance losses only 5% after 8,000 consecutive cycles at 100 mV s^{-1}.[80] The integrated electrochemical performances of the amorphous hydroxide were totally commensurate with those of $Co(OH)_2$ materials with crystalline phase.

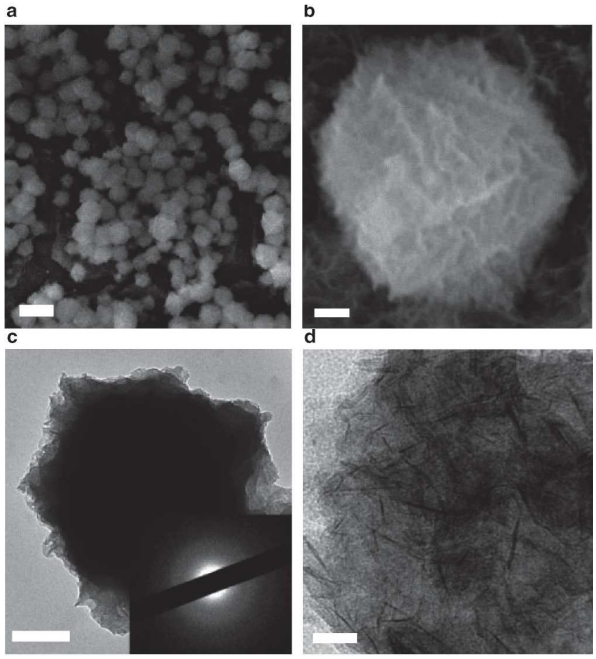

Fig. 6 (a,b) SEM images of the amorphous $Ni(OH)_2$ samples synthesized on graphite electrodes. (**c**,**d**) TEM images of the amorphous $Ni(OH)_2$ samples (the inset shows the corresponding selected-area electron-diffraction

pattern). Scale bars, 1 μm (a), 100 nm (b), 0.2 μm (c) and 20 nm (d). Reprinted with permission from Ref. 79a. Copyright (2013) Nature Publishing Group.

2.3 The composites containing Ni-, Co- hydroxides and carbon materials

The major issues for metal hydroxides (Ni- and Co- hydroxides) are their poor electrical conductivity and volume expansion during charge-discharge cycles especially for high-rate applications. Therefore, considerable work has been performed in order to improve the electrochemical properties by tuning their morphologies at nanoscale and modifying them to be nano-composites with some conductive materials. An efficient method is to make a hybrid containing both metal hydroxide and conductive material such as graphene, carbon black, and carbon nanotubes. For these carbon materials, their capacitance primarily relies on electrical double-layer mechanism without the involvement of Faradic process. Therefore, despite their high charge/discharge cycling stability and power density, most carbon materials still suffer from a lower specific capacitance than transition metal hydroxides or oxides. To further increase the energy density of hydroxide materials, several kinds of carbon materials have been selected and incorporated into metal hydroxides to form a pseudocapacitive composite.

Though $Co(OH)_2$ is considered as an important transition metal hydroxide for ECs, it displays less satisfactory electrochemical capacity and reversibility, compared with ruthenium oxides. Many composites containing $Co(OH)_2$, such as $Co(OH)_2$/carbon,[81] and $Co(OH)_2$/graphene [82-83] were prepared and thus the electrochemical properties of the composite was improved accordingly. The utilization percentage of $Co(OH)_2$ increases in the composite, the carboneous support of $Co(OH)_2$ yields a high conductivity and is beneficial to improvement of rate capability. So, the composite consisting of $Co(OH)_2$ and carbon support will greatly improve the capacitance value.

Graphene (or reduced GO) is a novel carbon material with 2D structure and has attracted intense interest in ECs electrode due to its unique electrical and mechanical properties. The addition of reduced GO (rGO) sheets is expected to provide a large support surface area for metal hydroxide nanocrystals and to improve the conductivity of the resultant composite materials. Zhu *et al.* prepared graphene/$Co(OH)_2$ composite employing Na_2S solution as both depositing and reducing agent.[84] The composite had a remarkable specific capacitance of 972.5 F g^{-1}, leading to a significant improvement in relation to each individual counterpart (137.6 and 726.1 F g^{-1} for graphene and $Co(OH)_2$, respectively). Aggregation would occur possibly resulting in a lower utilization of $Co(OH)_2$ active material in the case of being dried. The decoration of graphene nanosheets (GNS) with $Co(OH)_2$ nanoparticles could effectively inhibit the aggregation, resulting in a higher utilization of $Co(OH)_2$ and an improved electrochemical performance. The specific capacitance of the rGO/$Co(OH)_2$ composite prepared by solution method (as shown in **Fig. 7**) could reach 474 F g^{-1} at a current density of 1 A g^{-1} and this value could even retain 300 F g^{-1} at a high current density of 10 A g^{-1}, showing a relatively good rate capability. Meanwhile, the specific capacitance of the electrode still remained 90 % after 1,000 times of cycling, showing a good cycle stability.[85] All above reports indicate that the enhancement of capacitive performances can be attributed to the synergistic effect between graphene and $Co(OH)_2$ components in the composite.

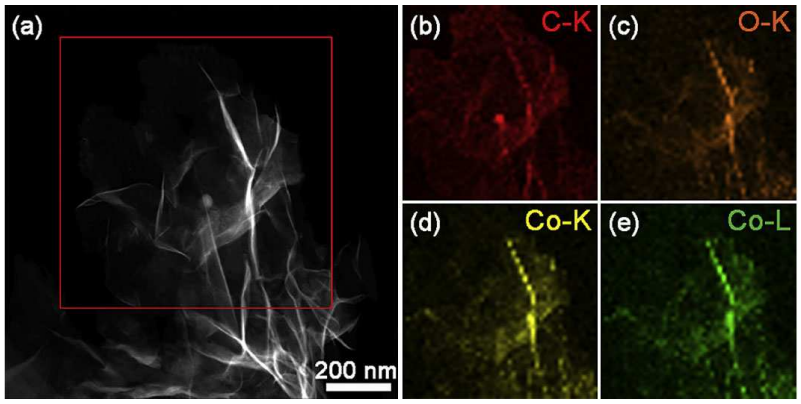

Fig. 7 STEM image (a), and carbon (b), oxygen (c), and cobalt (d, e) element mapping images of rGO/$Co(OH)_2$ composite. Reprinted with permission from Ref. 85. Copyright (2013) Elsevier B. V.

$Ni(OH)_2$ is of particular interest as ECs materials because it is a cheap material with high theoretical specific capacitance, however, one major drawback for $Ni(OH)_2$ is also its poor conductivity (~10^{-17} S cm^{-1}). A strategy to improve the electrochemical performance of $Ni(OH)_2$ is to combine it into a composite with an electronically conductive material. Many graphene/Ni hydroxide based composites have been successfully prepared, in which graphene or reduced GO improves the conductivity of the electrode materials.[86-94] Single-crystalline $Ni(OH)_2$ hexagonal nanoplates grown on graphene sheets showed a high specific capacitance (~1335 F g^{-1} at a charge and discharge current density of 2.8 A g^{-1}) and remarkable rate capability, significantly outperforming $Ni(OH)_2$ nanoparticles grown on GO and $Ni(OH)_2$ nanoplates simply mixed with graphene sheets,[95] as reported by Dai and shown in **Fig. 8**. Many functional groups of GO (hydroxyl, epoxy, carboxyl and carbonyl groups) could act as anchor sites for $Ni(OH)_2$ crystals growth. Thus, $Ni(OH)_2$/graphene composite prepared by electrostatic method showed superior electrochemical properties including high specific capacitance (1503 F g^{-1} at 2 mV s^{-1}) and excellent cycling stability up to 6,000 cycles even at a high scan rate of 50 mV s^{-1}.[96] This was attributed to its tailored properties, which were vital to the operation of ECs, including the intimate bindings, high conductivity, structural stability, and good wettability.

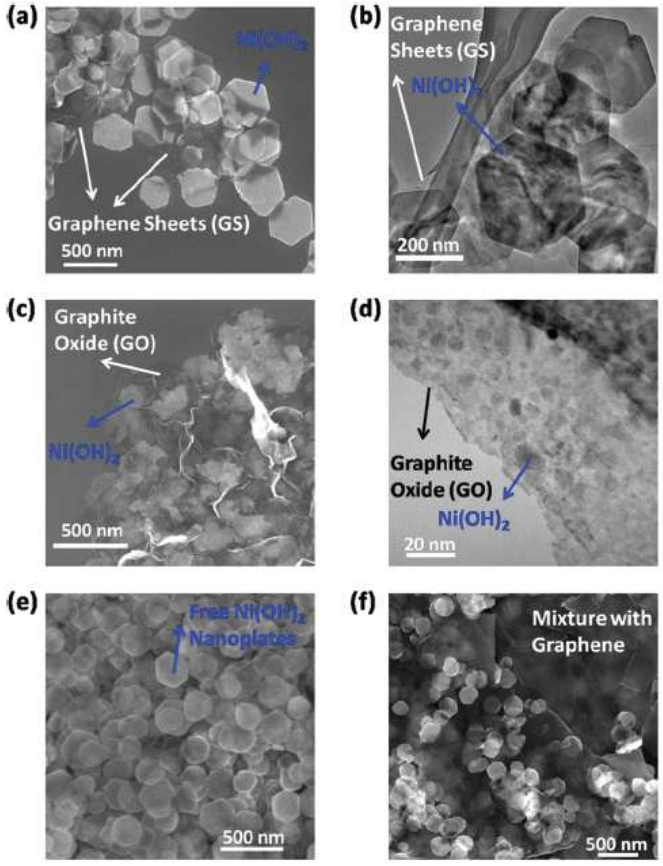

Fig. 8 SEM and TEM characterizations of $Ni(OH)_2$/GS composite, $Ni(OH)_2$/GO composite, and $Ni(OH)_2$ + GS physical mixture. (a) SEM image of $Ni(OH)_2$ nanoplates grown on GS. (b) TEM image of $Ni(OH)_2$ nanoplates grown on GS. (c) SEM image of $Ni(OH)_2$ nanoparticles grown on GO. (d) TEM image of $Ni(OH)_2$ nanoparticles grown on GO. (e) SEM image of $Ni(OH)_2$ hexagonal nanoplates grown in free solution (without graphene). (f) SEM images of simple physical mixture of presynthesized free $Ni(OH)_2$ nanoplates and GS. Reprinted with permission from Ref. 95. Copyright (2010) American Chemical Society.

In addition to graphene and reduced GO, carbon nanotubes (CNTs) are also suitable conductive supports for $Ni(OH)_2$ material.[97] Holze and co-workers developed a "bottom-up" chemical method to coat nanocrystalline $Ni(OH)_2$ onto the outer surface of multiwalled CNTs (MWCNTs) for flexible ECs electrodes, where the high electronic conductivity of CNTs permitted their use as the supporting backbone onto which $Ni(OH)_2$ could be deposited,[98] as exhibited in **Fig. 9**. The high capacitance and excellent rate capability of $Ni(OH)_2$/CNT electrodes could be attributed to the unique materials structure, where sponge-like $Ni(OH)_2$ nanoparticles were supported on a high-packing density, porous multiwalled CNT network with adequate access to electrons and ions in the electrolyte. $Ni(OH)_2$/CNTs composites could be also prepared by using electrochemical deposition method. The specific capacitance of the nanocomposite $Ni(OH)_2$/CNTs electrode was as high as 2486 F g^{-1} and stable over long cycling.[99] Meanwhile, active carbon could be also used to combine with $Ni(OH)_2$ to make an improvement in electrochemical performance.[100]

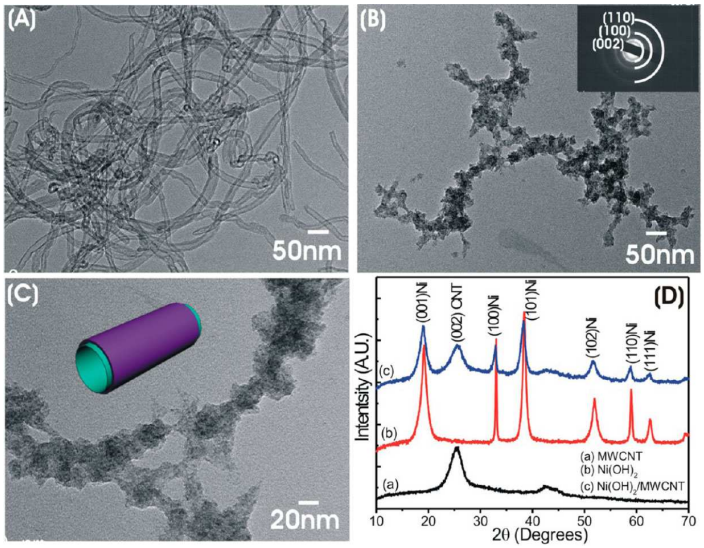

Fig. 9 TEM images of (A) pristine MWCNT and (B–C) $Ni(OH)_2$/MWCNT (30 mg cm^{-2}) and (D) XRD patterns of MWCNTs, $Ni(OH)_2$, and $Ni(OH)_2$/MWCNTs powders. Reprinted with permission from Ref. 98. Copyright (2013) American Chemical Society.

Zhao *et al*. first demonstrated the preparation of 3D CNT-pillared rGO sheets with embedded $Ni(OH)_2$ nanoparticles for pseudocapacitor applications, where CNTs with embedded $Ni(OH)_2$ nanoparticles as pillars for rGO sheets. The composite displayed specific capacitances as high as 1235 and 780 F g^{-1} at current densities of 1 and 20 A g^{-1}, respectively.[101] Graphene/$Ni(OH)_2$ composites could be also prepared by a scalable solid-state reaction method. The resulting composites with well-dispersed $Ni(OH)_2$ nano-particles on rGO surface showed a high specific capacitance of 1568 F g^{-1} and good cycling stability (>75% retention for 1,000 cycles) at a current density of 4 A g^{-1} in 1 M KOH.[102]

3. Bimetallic hydroxide

Nickel hydroxide is deemed as one of the most promising electrode materials owing to its high theoretical specific capacitance, up to 2358 F g^{-1}. However, its such high capacitance is hard to be realized in practice owing to its poor conductivity. It has been reported that the incorporation of cobalt into nickel hydroxide can significantly improve the electrochemical and conducting properties of the overall electrode material, due to the formation of highly conductive CoOOH during the charge-discharge process.[103] Thus, various nickel-cobalt double hydroxides electrodes have been prepared, and their enhanced electrochemical performances have been also reported.[104-121]

3D porous Ni-Co binary hydroxides are intensively studied due to their high specific surface area and porous structure. Urchin-like $Ni(OH)_2$–$Co(OH)_2$ hollow microspheres could be synthesized by microwave-incorporated hydrothermal method.[122] The hollow microspheres achieved a high specificcapacitance of 2164 F g^{-1} at 1 A $g^{-1}$and long-term cycle life. $Co_{0.5}$-$Ni_{0.5}$ hydroxide nanocones could deliver a specific capacitance of 1580 F g^{-1} at a galvanic current density of 10 A g^{-1}, measured from charge-discharge curves. The authors attributed it to the enhancement of the electro-active sites participated in the red-ox reaction due to possible valence interchange or charge hopping between Co and Ni cations.[106] Hollow rhombic dodecahedral

Ni-Co hydroxides nanocages which were composed of thin nanoplatelets could be synthesized using ZIF-67 nanocrystals as templates. The porous nanocages exhibited superior pseudocapacitance properties due to their novel hierarchical and submicroscopic structures.[111,113]

Ni-Co double hydroxides films also show a great potential in ECs electrode. A high specific capacitance of 2682 F g^{-1} at 3 A g^{-1} based on active materials was obtained using Ni-Co layered double hydroxides (LDHs) hybrid film on nickel foam.[104] $Co_{0.72}Ni_{0.28}$ double hydroxides deposited on stainless steel by potentiostatic deposition method had the highest specific capacitance of 2104 F g^{-1} in 1 M KOH.[114] The composition ration of Ni-Co had a great influence on the morphology of double hydroxide arrays deposited on stainless steel, where Ni:Co = 2:1 achieved a specific capacitance of 456 F g^{-1} with an energy density of 12.8 Wh kg^{-1}.[109] The nanocrystalline $Co_{1-x}Ni_x$ hydroxides thin films prepared by potentiodynamic deposition possessed different porous, nanoflake like morphology and superhydrophilic behavior by the composition influence. The maximal specific capacitance for Ni-Co hydroxides electrode was found to be about 1213 F g^{-1} for the composition $Co_{0.66}Ni_{0.34}$ LDHs in 2M KOH electrolyte at 5 mV s^{-1} scan rate.[116]

Zwitterionic p-aminobenzoate intercalated α-hydroxides of nickel and cobalt could be synthesized by ammonia precipitation and they were shown to exfoliate in water. The monolayers from a mixture of the aqueous colloidal dispersions of the α-hydroxides could be co-stacked instantaneously by the addition of nitrate anions to give hybrids in which the two hydroxide layers were interstratified, as schematically shown in **Fig. 10**. The hybrid hydroxides having 80% nickel hydroxide showed the best electrochemical performance with a high specific capacitance of 990 F g^{-1} and very good cycling stability.[123]

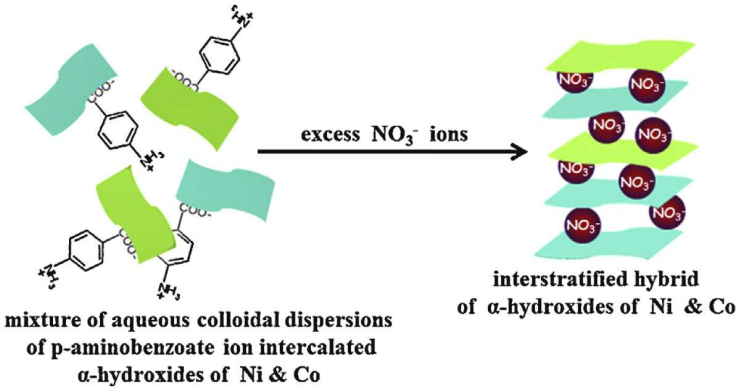

Fig. 10 Schematic representation of the preparation of the nitrate intercalated interstratified a-hydroxide hybrids. Reprinted with permission from Ref. 123. Copyright (2013) Elsevier Ltd.

Ni-Co double hydroxides deposited on ZnO nanowire arrays [108] and zinc tin oxide nanowires [107] could demonstrate outstanding performances with a specific capacitance of 1624 and 1805 F g^{-1}, respectively. Li *et al.* also found that the atomic ratio between Co and Ni had a significant effect on their electrochemical activities. The specific capacitance of 2614 F g^{-1} was achieved when the atomic ratio of Co to Ni was 0.57 : 0.43.[110] Ni-Co binary hydroxide systems with controllable morphologies from nanosheets, to nanoplates-nanospheres, to nanorods, and to a nanoparticle geometry by simply tailoring the Ni and Co cation ratios in the initial reactants was reported by Lian.[124] The drastically different morphologies significantly affected the

electrochemical performance of the binary hydroxides as electrode materials. A high capacitance of 1030 F g^{-1} was achieved for the nanorod morphology at the current density of 3 A g^{-1}.[124] Even the lattice spacing and crystal size of Co-Ni hydroxide nanosheets could be slightly tuned by the metal ratio.[125] Though the optimum Co/Ni ratios are different in the above reports due to different preparation methods, we can still draw a conclusion that bimetallic hydroxide of Ni-Co are super to their individual components to a large extent.

Liu *et al*. developed an accumulative approach to move beyond simple incorporation of conductive carbon nanostructures to improve the performance of metal hydroxides. Ni-Co double hydroxide/graphene composites were first synthesized by co-precipitation, and then they were assembled into films by integrating with few walled CNTs that could be directly used as electrode, as shown in **Fig. 11**. With 50% Co and 50% Ni, the composite exhibited a remarkable maximum specific capacitance of 2360 F g^{-1} at 0.5 A g^{-1}. The control experiments showed that the double hydroxides outperformed either $Co(OH)_2$ or $Ni(OH)_2$ alone,[126] proving that graphene could greatly boost the electron transfer during the red-ox reaction.[127]

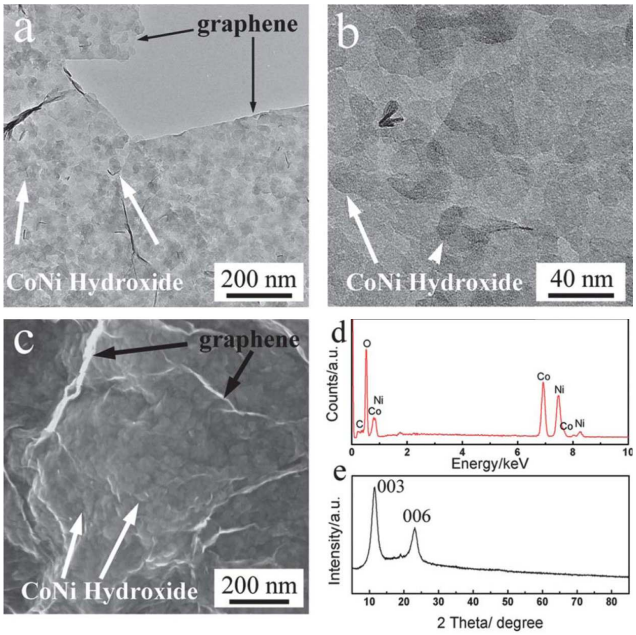

Fig. 11 Material characterization of the $Co_{0.5}Ni_{0.5}(OH)2$/graphene composite: (a) and (b) TEM images at different magnifications; (c) SEM image; (d) EDS spectrum and (e) XRD pattern. Taken from Ref. 126 with permission from RSC Publications.

More recently, Ni–Cu double hydroxide spheres was synthesized by chemical bath deposition method on different substrates including copper-, nickel-foam, and carbon paper. When the substrates changed from a copper foam to a nickel foam or carbon paper, the deposited material became pure nickel hydroxide with a flower-like morphology. The Ni-Cu double hydroxide also demonstrated a high specific capacitance of 1970 F g^{-1}.[128]

4. Hydrotalcite-like compounds

4.1 Layered double hydroxides

Layered double hydroxides (LDHs) are a kind of lamellar compounds made of positively

charged brucite-like layers and an interlayer region containing compensating charge anions and salvation molecules. The most widely studied LDHs usually contain both divalent and trivalent metal cations. A general formula for LDHs can be written as, $[M^{2+}_{1-x}M^{3+}_{x}(OH)_2][A^{n-}]_{x/n}\cdot zH_2O$, where M^{2+} may be common, such as Mg^{2+}, Zn^{2+}, Co^{3+}, or Ni^{2+} and M^{3+} may be Al^{3+}, Ga^{3+}, Fe^{3+}, or Mn^{3+}. A^{n-} is a charge compensating inorganic or organic anion, *e.g.* CO_3^{2-}, Cl^-, SO_4^{2-}, and x is normally between 0.2-0.4. Due to the flexible ion-exchangability and easily tunable composition, LDHs have a series of important applications in catalyst or catalyst precursors, anion exchangers, precursors to other materials and so on. For some earth-abundant transition elements including Co, Ni, Mn and Fe can be used as the building blocks of LDHs layers and there are wide and flexible galleries between host layers, these LDHs have also been applied as electrode materials in ECs due to these LDHs nanosheets facilitating increased surface area and remarkably decreased diffusion distances for ions.[129] The simplest and most commonly method to prepared LDHs is co-precipitation of the chosen M^{2+} and M^{3+} hydroxides with diluted NaOH and/or Na_2CO_3 or $NaHCO_3$. However, they can also be synthesized using urea hydrolysis, hydrothermal or ion-exchange method, *etc*. Nickel and cobalt are the most commonly studied two elements in these systems due to their abundance and high capacitance.

To obtain excellent capacitive materials, they should be of a large surface area and highly ordered dimensions. Thus, three common approaches can be taken in account to realize this goal. Firstly, larger specific surface area of active materials can accommodate more electrolyte ions for red-ox process. Secondly, providing a suitable mesopore structure is important for the mass transfer of electrolytes. Finally, electroactive materials with a high electrical conductivity can deliver a high capacitance under a high discharge current density, exhibiting an excellent high rate capability. Based on above analysis, there are several points are intensively investigated by scientists. Mousty *el al.* found that the electrochemical behavior of Ni-rich LDH was mainly governed by an electron hopping mechanism, whereas in CoAl-LDH a multi-site pseudo-capacitive behavior was observed.[130]

4.1.1 Co-Al layered double hydroxides

Among various LDH materials, CoAl-LDH was prominent due to its high specific capacitance and various production methods.[130-132] Yang *et al.* prepared a continuous CoAl-LDH nanosheet thin-film electrode by drying a nearly transparent colloidal solution of LDH nanosheets on an ITO substrate.[133] The partial isomorphous substitution of Co^{2+} by Al^{3+} is the key factor in the improvement of the electrochemical behavior, because the Al^{3+} favors the retention of the original layered structure during the red-ox reaction. The $Co_{0.75}Al_{0.25}$-LDH thin-film electrode had a large specific capacitance of 2500 F cm^{-2} (833 F g^{-1}) with a good high-rate capability.[133] Multilayer films composed of two kinds of one-atom-thick sheets, GO and CoAl LDHs *via* layer-by-layer assembly was performed by Jin group,[134-135] the hybrid films had well organized layered structure as well as with finely controlled film thickness and uniformity, as presented in **Fig. 12**. The obtained CoAl LDHs/GO films displayed a long cyclic life and an extremely high specific capacitance up to 1200 F g^{-1} under a scan rate of 5 mV s^{-1} after reducing the GO to reduced GO.[134-135] The films fabricated by this method also could be transferred to polyethylene terephtalate substrate to produce a flexible EC device.

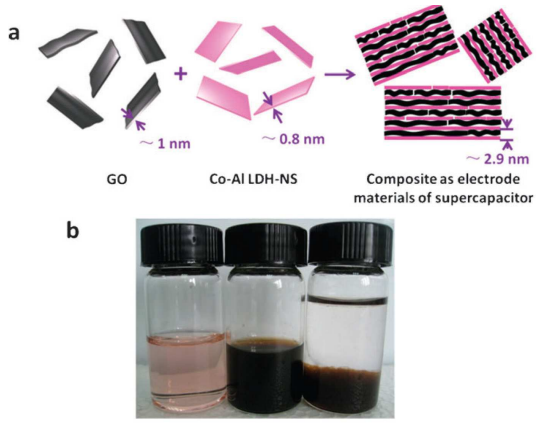

Fig. 12 (a) Schematic of the formation and structure of Co-Al LDH-NS/GO composite. (b) digital photographs of (left) an aqueous dispersion of Co-Al LDH-NS, (middle) an aqueous dispersion of GO, and (right) a mixture of Co-Al LDH-NS and GO. Taken from Ref. 134 with permission from RSC Publications.

However, when Co-Al LDHs were soaked in KOH solution, Al^{3+} ions would be leached off from the lattice, making them transform into β-$Co(OH)_2$, degrading the electrochemical performance of electrode. The transformations were influenced by the Co/Al ratio, soak temperature, alkali concentration and also took place during the charge/discharge process.[136] The dissolution of $Al(OH)_3$ in the electrolyte and /or surface modification of Y, Er or Lu could improve the cycling charge-discharge performance, because they could retard the transformation from LDH into β-$Co(OH)_2$.

CoAl LDHs usually suffered from low rate and poor cycling stability at high current densities. In order to deal with these drawbacks, one strategy is doping LDHs with other carbon materials. By coating CoAl LDHs with conductive film or self-assembling them onto graphene or other conductive supports can greatly improve its high-current capacitive behavior.[137-139] The formation of Co-Al LDHs on the graphene nanosheets could prevent the restacking of the as-reduced graphene nanosheets,[140-141] as depicted in **Fig. 13**. Zhang *et al.* applied refluxing method with urea as a basic precipitant to prepare graphene/CoAl-LDH for 48 hours, where the CoAl-LDH crystals adhered to the surface of graphene nanosheets to form laminated structure with smaller size compared with the pure CoAl-LDH, which facilitated electrolyte soaking into electrode materials.[139] A time saving method is microwave-assisted irradiation, the reaction time can be greatly reduced to about 2 hours.[142]

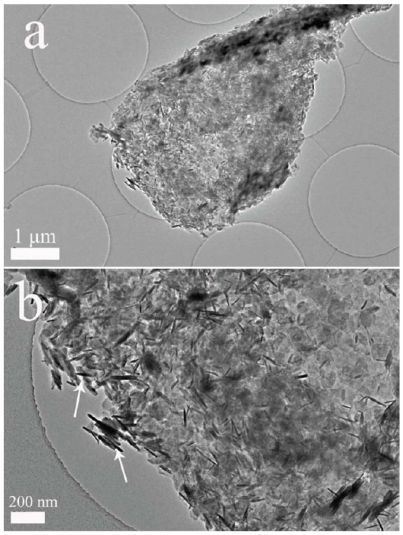

Fig. 13 (a) Low and (b) high magnification TEM images of nanosized LDHs/GO hybrid at high LDHs nuclei concentration. Reprinted with permission from Ref. 140. Copyright (2012) American Chemical Society.

CoAl-LDH@poly(3,4-ethylenedioxythiophene)(PEDOT) core/shell nanoarray was grown on a flexible Ni foil substrate.[138] Its performances were superior to those of conventional LDH arrays without the PEDOT coating. The enhanced pseudocapacitor behavior of the LDH@PEDOT electrode was related to the synergistic effect of its individual components. The LDH nanoplatelet core provided abundant energy storage capacity, while the highly conductive PEDOT shell and porous architecture facilitated the electron/mass transport in the red-ox reaction.[138] Pt films coated CoAl LDH arrays also exhibited enhanced electrochemical properties.[137]

4.1.2 Ni-Al layered double hydroxides

NiAl-LDH materials are another kind of LDHs that have been extensively used as electrode materials of supercapacitor.[130,143-146] They have shown greatly potential in EC applications as highly red-ox active, low-cost and environmentally benign materials.[147]

Core–shell NiAl LDH microspheres with tunable interior architecture have been fabricated and reported by a facile and cost-effective *in situ* growth method on Si microsphere, as presented in **Fig. 14**. The hollow NiAl-LDH microspheres with the highest surface area (124.7 m^2 g^{-1}) and a mesopore distribution (3-5 nm) could give a maximum specific capacitance of 735 F g^{-1} and good cycle performance, as well as remarkable rate capability.[148]

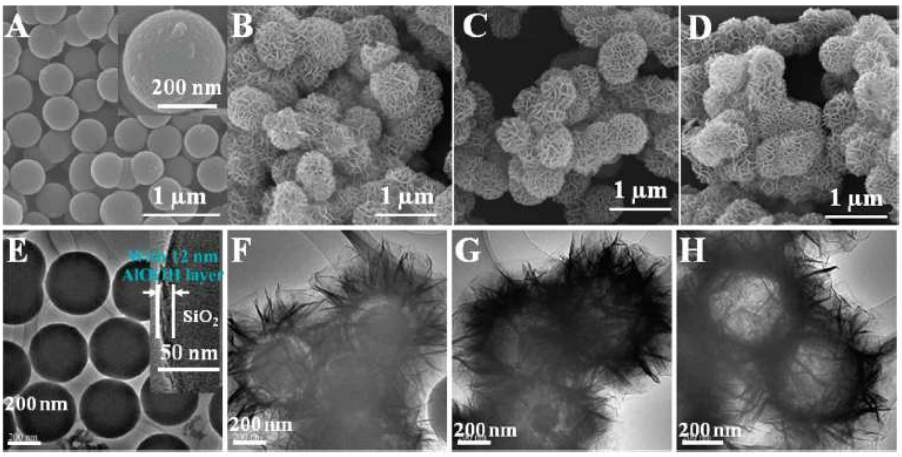

Fig. 14 TEM and SEM images of (A, E) SiO_2/AlOOH microspheres; (B, F) SiO_2/NiAl-LDH core−shell microspheres; (C, G) SiO_2/NiAl-LDH yolk−shell microspheres; (D, H) NiAl-LDH hollow microsphere. Reprinted with permission from Ref. 148. Copyright (2012) American Chemical Society.

Though the capacitance of NiAl LDHs up to 1000 F g^{-1} have been reported in various electrolytes, but they often suffer from low electrical conductance and short cycle life during application. Some efforts have been thus made to improve the performance of them by creating conductive nanostructures supported NiAl LDHs,[149-155] as shown in **Fig. 15**. The incorporation of Ni-Al LDH platelets onto graphene can prevent the restacking of graphene nanosheets (GNS) and improve the capacitance of the composite electrode, the electrolyte/electrode accessibility and the conductivity.[156-157] The prepared GNS/LDH composite exhibited a high specific capacitance (781.5 F g^{-1} at 5 mV s^{-1}) and excellent long cycle life.[158] Using GNS as a support, the GNS/NiAl-LDH composite had been successfully prepared by liquid phase deposition method as an electrode material for ECs. Due to the improvement of conductivity and adhesion, facile electrolyte penetration and better Faradic utilization of the electro-active porous surface, the as-obtained GNS/NiAl-LDH composite showed a considerably improved electrochemical performance with a specific capacitance of 1255.8 F g^{-1}.[159] Alternative method was using layer-by-layer deposition of AlOOH onto GNS followed by an *in situ* growth process of NiAl-LDHs to form an interesting sandwich structure,[160-161] and the composite had a specific capacitance of 1329 F g^{-1} at a current density of 3.57 A g^{-1}.

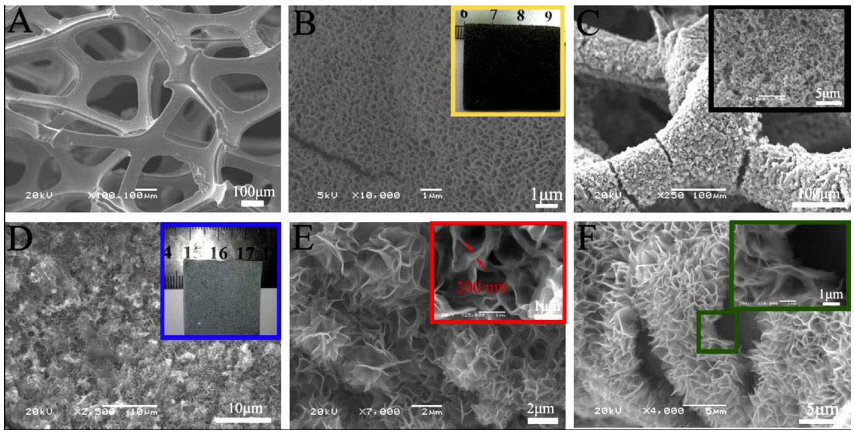

Fig. 15 (A) SEM image of Ni foam; (B) SEM image and digital photo (inset in Fig. 15B) of NiOOH; (C) Small

and large (inset in Fig. 15C) SEM images of DOS-LDH; (D, E) SEM images and digital photo (inset in Fig. 15D) of Ni-Al LDH; (F) Lateral view image of Ni-Al LDH. Reprinted with permission from Ref. 151. Copyright (2013) Elsevier B.V.

Delaminated Ni-Al LDHs could be also incorporated between graphene nanosheets to form a layered hybrid structure as a new supercapacitor electrode material, as reported by Wimalasiri,[162] GO and delaminated Ni-Al LDH in aqueous medium—instead of the *in-situ* growth of Ni-Al LDH on GO nanosheets. Both materials in their layered form would provide more contact between electrochemically active areas and result in favorable conditions to realize their electrochemical energy storage capacity. The graphene/Ni-Al LDH–based electrodes provided a specific capacitance of 915 F g^{-1} at a current density of 2 A g^{-1}.[162]

Similarly to CoAl-LDHs, when a layered double hydroxide, $[Ni_4Al(OH)_{10}]NO_3$ was aged at 60 °C in a concentrated KOH solution (around 7 mol L^{-1}), it transformed into β-form $Ni(OH)_2$; when it was cycled electrochemically, it could also transform into β-$Ni(OH)_2$ but finished much soon, which leaded to the decrease of the maximal number of exchanged electron per nickel atom as the charging/discharging cycling was continued and a degradation of the electrodes. The well-crystallized β-$Ni(OH)_2$ had a worse electrochemical activity than NiAl-LDHs. However, its high temperature performance could be improved by lowering the concentration of electrolyte and /or adding rare metal oxides such as Lu_2O_3, Er_2O_3 or Y_2O_3.[163]

4.1.3 Other layered double hydroxides

In addition to CoAl-, NiAl-LDHs as popular electrode materials of ECs, various other LDHs have been also reported as electrode materials. Xu *et al.* found that the specific surface area of $M^{II}_2M^{III}$-LDH (M^{II}: Co and Mn; M^{III}: Al and Fe) strongly affects their capacitance, but these LDH materials exhibited a not high specific capacitance (normally 100-200 F g^{-1}) at a scanning rate of 1 mV s^{-1} in 6 M KOH solution.[164] The exfoliation of $Mn^{II}Al^{III}$ sulfonate and sulfate LDHs and their combination with GO by charge-directed self-assembly were reported.[165] Exfoliation of the bulk material in formamide yielded colloidal suspensions of positively charged LDH nanosheets with lateral dimensions of tens to hundreds of nanometers and thicknesses down to 1.3 nm. The hybrid material were tested for ECs and showed significant increase compared to the pristine material.

CoMn-LDH nanowalls were deposited on flexible carbon fibers (CF) *via* an *in situ* growth approach. The resulting CoMn-LDH/CF electrode could deliver a high specific capacitance (1079F g^{-1} at 2.1 A g^{-1} normalized to the weight of the active LDH material) with excellent rate capability even at high current densities (82.5% capacitance retention at 42.0 A g^{-1}).[166] The dramatic performance is mainly attributed to the homogeneous and ordered dispersion of metal units within the LDH framework, which enriches the red-ox reactions associated with charge storage by both Co and Mn.

Magnetic films of CoFe-LDH nanoplates and porphyrin anions were fabricated by the layer-by-layer technique with the assistance of an external magnetic field, which showed enhanced electrochemical behavior.[167] Hwang group reported Zn-Co-containing LDH phases and their exfoliated and calcined derivatives. The Zn–Co-LDH materials showed not only interesting magnetic properties but also pseudocapacitance behavior with a discharge capacity of 160–170 F g^{-1} and a good capacitance retention.[168]

A NiTi-LDH thin film on nickel foam substrate was synthesized using two hydrothermal treatment steps with ammonia solution as a basic precipitant. NiTi LDH crystallites perpendicular to the surface of the nickel foam substrates was formed and Ti atoms were dispersed homogeneously in the LDH lattice. A high specific capacitance of 10.37 F cm^{-2} was achieved at a current density of 5 mA cm^{-2} and 86% of the initial specific capacitance was remained after 1000 cycles.[169] Ni-V LDH composites were prepared by co-precipitation process, during which small amounts of vanadium sources were decomposed by acid solution and mixed with β-$Ni(OH)_2$, and then a small quantity of nickel hydroxides transformed gradually to Ni-V LDH composite. Compared to flake-like β-Ni(OH)2, the Ni-V LDH composite exhibits a much higher specific capacitance of 2612 F g^{-1} at the scan rate 2 mV s^{-1}.[170]

Other LDHs such as CoCr, CoIn LDHs were also investigated as electrode materials of ECs with a good stability. However, their specific capacitance was not high.[171]

The hierarchical structure composed of NiMn-LDH microcrystals grafted on CNTs backbone was prepared by Zhao and colleague by chemical deposition,[172] as shown in **Fig. 16**. The unique NiMn-LDH/CNT core-shell heterostructure could be evidenced by SEM and TEM images. The NiMn-LDH played the role of electrochemically active species while carbon nanotubes served as both support and electron collector. Electrochemical measurement showed that the Ni_3Mn_1-LDH/carbon nanotube electrode was rather active, delivering a maximum specific capacitance of 2960 F g^{-1} (at 1.5 A g^{-1}), together with good rate capability and excellent cyclability. Flexible ECs with asymmetric configuration could be fabricated using NiMn-LDH film and rGO/CNTs film as the positive and negative electrode, respectively, exhibited a wide cell voltage of 1.7 V and large energy density of 88.3 Wh kg^{-1}.[172]

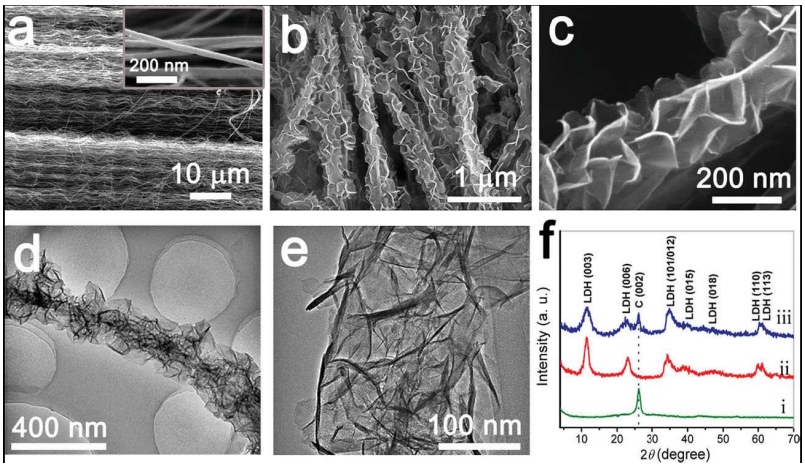

Fig.16 (a) SEM image of the pristine CNT (inset: the enlarged image). (b,c) SEM images and (d,e) TEM images of the NiMn-LDH/CNT. (f) XRD patterns of: (i) the pristine CNT, (ii) the powdered sample of NiMn-LDH, (iii) the NiMn-LDH/CNT. Reprinted with permission from Ref. 172. Copyright (2014) Wiley-VCH.

CoNiAl three-component LDHs with hydrotalcite-like structure could be successfully synthesized by homogenous precipitation using urea as a precipitant, whose capacitive behavior was influenced by the Co/Ni atomic ratio and electrolyte. When the molar ratio of Co/Ni reached 5, CoNiAl LDH displayed the best capacitive performances.[173] The $Co_{0.55}Ni_{0.13}Al_{0.32}$ LDH delivered more specific capacitance in 1 M KOH than in 1 M LiOH or NaOH. Increasing the concentration of KOH from 1 to 6 M, the specific capacitance was elevated from 644 to 1124 F

g^{-1} at 1 A g^{-1}. After 1,000 continuous charge/discharge cycles at 2 A g^{-1}, $Co_{0.55}Ni_{0.13}Al_{0.32}$ LDH exhibited a good capacitance retention (93.3%).[173] When ternary-component NiCoAl LDHs nanosheets and CNT composites were fabricated using urea precipitation, the small size CNTs would well be incorporated into the network of LDHs nanosheets to form a homogeneous hybrid, as shown in **Fig. 17**. The specific capacitance could reaches 1035 F g^{-1} at a current density of 1 A g^{-1}, which increased by 33.3% in comparison to that of pure NiCoAl-LDH nanosheet.[174] In addition to precipitation, NiCoAl-LDH nanosheets with anisotropic morphology could be also synthesized by potentiostatic deposition, and their composition could be easily changed.[175]

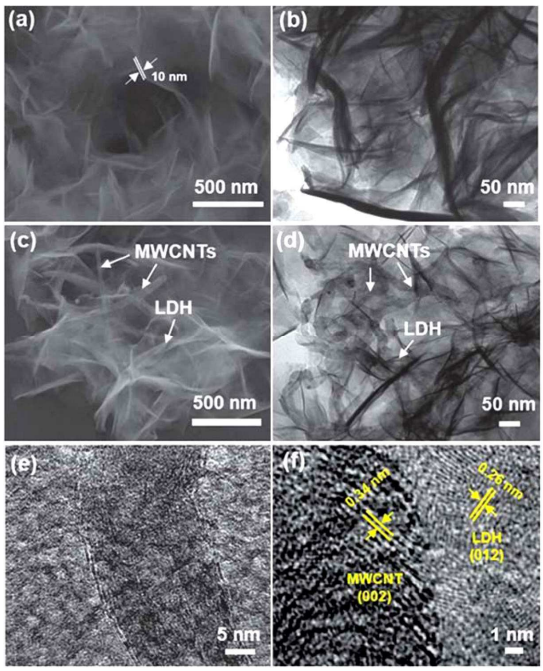

Fig. 17 FE-SEM and TEM images of (a and b) the NiCoAl-LDH nanosheets and (c and d) the NiCoAl-LDH–MWCNTnanohybrids, and high-resolution TEM images of (e and f) the NiCoAl-LDH–MWCNT nanohybrids. Taken from Ref. 174 with permission from RSC Publications.

Well dispersed Li-Al LDHs could be synthesized by solvothermal approach by adjusting the concentration of ethanol. The hexagonal Li-Al LDHs calcined at 450 °C exhibited the specific capacitance of 848 F g^{-1} at a current density of 1.25 A g^{-1}.[176]

4.2 α-cobalt hydroxide

Cobalt hydroxide is well known to crystallized in two polymorphs, *i.e.* the metastable α-type and thermodynamically stable β-form. The previous one is isostructural with a hydrotalcite-like structure consisting of positively charged $Co(OH)_{2-x}(OH)_x$ layers and charge balancing anions in the space between hydroxide layers. Its structure is superior to β-form for electrochemical reactions because of its poorly and turbostratically crystallized structure, large interlayer spacing. These α-type $Co(OH)_2$ materials used for EC can be prepared by co-precipitate,[177-181] hydrothermal method,[182-185] electrodeposition,[186-194] ionothermal synthesis,[195] γ-ray irradiation,[196] and so on. Biomolecule-assisted method can be applied to synthesize 2D nanoporous α-$Co(OH)_2$ mesocrystal nanosheets, where the amino acid L-arginine played a dual role. It acted as an hydrolysis-controlling agent whilst stabilizing the synthesized $Co(OH)_2$ nanocrystallite building

blocks.[183]

The intercalated anions are exchangeable for α-$Co(OH)_2$, thus making it possible to adjust the interlayer spacing. Through an anion exchange reaction, the interlayer spacing and intercalated anions in α-$Co(OH)_2$ layers can be changed. Hu *et al.* reported that the intercalated anions in α-$Co(OH)_2$ had a critical effect on the basal plane spacing, morphology and specific capacitance.[197] Jin *et al.* also found that the interlayer space and electrochemical activity of α-$Co(OH)_2$ were closely related and that larger interlayer spacing allowed more electrolyte ions to be stored, leading to a higher electrochemical activity.[198]

However, the low conductivity of $Co(OH)_2$ usually limits its high-rate capabilities. The hybrid synthesis of α-$Co(OH)_2$ on conductivity ITO nanowires forming nanoscale heterostructures could lead to improved high-rate capabilities, originating from the enhanced electrode and electrolyte conductivities, where ITO nanowires improved electron conductivity without using carbon black and polymer binder.[199-201] Meanwhile, using α-$Co(OH)_2$ and conductive carbon composites was also effective to improve its electrochemical properties.[191,193] The CNTs grown on carbon substrates can offer an external surface area for supporting electroactive α-$Co(OH)_2$ materials, as presented in **Fig. 18**. Thus, nanometer-sized α-$Co(OH)_2$ sheets were attached to the CNTs/carbon paper substrates by using electrodeposition technique, as reported by Zhang *et al*.[190] The composite electrode showed a large specific capacitance of 1083 F g^{-1} at a current density of 0.83 A g^{-1} in 6M KOH, because the interconnected nanosheets of α-$Co(OH)_2$ facilitated the contact of active material with electrolyte. The presence of CNTs provide short path for ion/electron transfer and sufficient contact between materials and electrolyte.[190]

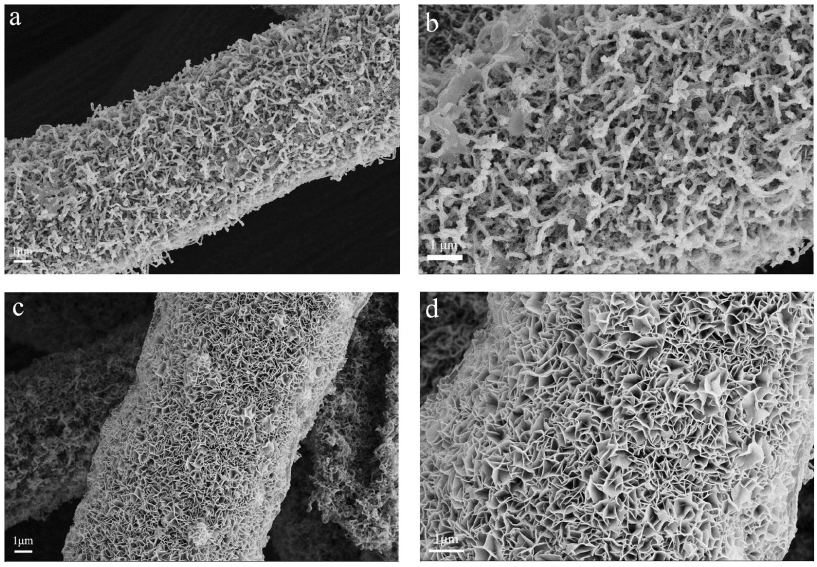

Fig. 18 SEM images of prepared $Co(OH)_2$ deposited at different times of 180 s (a, b) and 300 s (c, d). Reprinted with permission from Ref. 190. Copyright (2013) Elsevier Ltd.

Another method that can be adopted is using guest metal substitution to doping α-$Co(OH)_2$, such as Al and Zn.[179,189] Zn-substituted α-$Co(OH)_2$ nanosheet electrodes exhibited much better cycling performance than the pure α-$Co(OH)_2$ nanosheet electrode, as reported by He *et al*.[189] The sample with 21.1 at.% Zn substitution demonstrated a high cycling stability with a capacitance

loss of only 0.6% from 652 F g^{-1} after 2,000 cycles. Recently, exfoliating of α-$Co(OH)_2$ in formamide solution could form graphene-like 2D ultrathin α-$Co(OH)_2$ nanosheets. The exfoliated α-$Co(OH)_2$ ultrathin nanosheets had much better electrochemical properties than its precursor, including a high specific capacitance of 1280 F g^{-1}, remarkable rate capability, as well as good cycling stability.[180] The ultrathin nanosheets obtained by exfoliation are suitable for industrialization owing to the simple synthetic procedures and reaction conditions.[202]

However, α-$Co(OH)_2$ is metastable in structure and easily undergoes a phase transformation into the more stable β-counterpart in strongly alkaline media. When it was immersed in KOH solution for a long time, it would transform to β-$Co(OH)_2$ and Co_3O_4,resulting in a dramatic decrease in the specific capacitance.[203] To keep α-$Co(OH)_2$ stable in solution, inert atmosphere and week alkaline media are necessary.

4.3 α-nickel hydroxide

Similarly to cobalt hydroxide, nickel hydroxides also have two polymorphs, *i.e.*, α- and β-type $Ni(OH)_2$. α-hydroxides of nickel have a structure similar to LDHs. β-type is of the formula $Ni(OH)_2$ and it is an ordered stacking of neutral layers of the compound with an interlayer spacing of 0.46 nm. There have been extensively studied as they are widely employed as electrode materials of alkaline secondary batteries and supercapacitor.[204]

These methods used for preparation of α-$Ni(OH)_2$ materials that were used as electrode materials of supercapacitor included electrochemical deposition,[205-209] precipitation,[210-212] hydrothermal method,[213-217] *etc*. Microwave heating is another very useful technique that has been widely applied for the synthesis of inorganic compounds including α-$Ni(OH)_2$. Mesoporous α-$Ni(OH)_2$ material was reported to be produced in a large scale with assistance of microwave irradiation in 2.5 minutes in ethylene glycol solution.[218]

3D hierarchically structured α-$Ni(OH)_2$ materials are good candidates for electrode of ECs, the porous features facilitate easy transportation of electrolyte to reaction sites and lead to a further increase in the specific capacitance.[219] Hollow spheres of α-$Ni(OH)_2$ were fabricated by Wu using polystyrene sphere as template and electrochemical deposition, which showed greatly enhanced electrochemical performance in alkaline solution due to its opening structure.[207] Without using sacrificed templates, flower-like α-$Ni(OH)_2$ microspheres composed of nanowires could be prepared by a solvothermal method using triethylene glycol and water as the mixed solvent. Compared with other conventional solvents, such as glycerol, alcohol and water, triethylene glycol had a longer chain length, moderate polarity and viscosity. Thus, the crystalline products obtained in this triethylene glycol/H_2O solvent tended to have kinetically slower growth rate. The as-formed nanocrystals had enough time to rotate adequately and found the low-energy configuration interface. Then growth units with oriented growth direction were thus formed. These building blocks coalesced and aggregated together to form porous microspheres, as shown in the following **Fig. 19**. The sample had a high BET surface area of 318 m^2 g^{-1} and showed a high a specific capacitance of 1788.9 F g^{-1} at 0.5 A g^{-1} as well as excellent rate performance.[213]

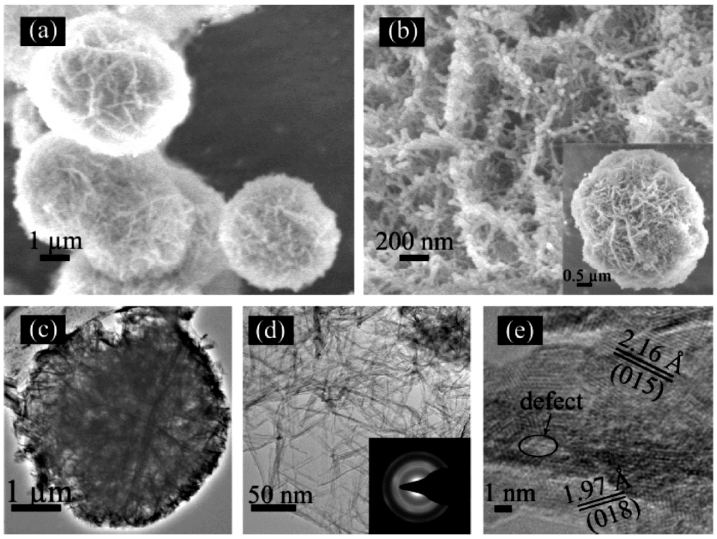

Fig. 19 (a,b) SEM and (c,d,e) TEM images of the microflower-like α-$Ni(OH)_2$. Reprinted with permission from Ref. 213. Copyright (2013) American Chemical Society.

One simple method to improve the electrochemical properties of α-$Ni(OH)_2$ materials is annealing them under an rational temperature. Porous flowerlike α-$Ni(OH)_2$ microspheres were synthesized by aqueous-phase reaction. Heating it under a moderate temperature, *i.e.* 200 °C could make it deliver the highest specific capacity of 1551 F g^{-1} in 6 M KOH, while a higher calcination temperature would decrease its capacitance due to the formation of NiO.[220] Yang *et al.* reported that annealing α-$Ni(OH)_2$ films on Ni foam at 100 °C would deliver a specific capacitance of 2447 F g^{-1}.[221] The improved capacitance was supposed to be resulted from the removal of physically absorbed water in α-$Ni(OH)_2$. Yu *et al.* found that flower-like NiO/α-$Ni(OH)_2$ composite had a superior pseudocapacitive performance than the individual α-$Ni(OH)_2$ and NiO, but poor electronic conductivity hindered its capacitance retention at high current density, where the composite was obtained by heating α-$Ni(OH)_2$ at 250 °C for different time. Another method can be adopted is guest elemental doping in α-$Ni(OH)_2$ crystals. Al and Zn doped α-$Ni(OH)_2$ materials were reported to be prepared by electrochemical deposition and hydrothermal method,[222-223] because them tended to formation of Ni-based LDHs.

However, the poor conductivity is the major drawback for $Ni(OH)_2$ as semiconductor material, leading to the poor rate capability of the electrode, as well as the low power output of ECs. An efficient route to overcome this shortcoming is supporting $Ni(OH)_2$ on carbon materials, among them CNTs is optimum.[224-226] α-$Ni(OH)_2$/graphite nanosheet composite was prepared *via* a homogeneous precipitation method to form a 3D hierarchical porous structure, of which fine a-$Ni(OH)_2$ nanocrystals as building blocks was formed directly on the matrix of graphite nanosheets. The composite exhibited the specific capacitance as high as 1956 F g^{-1} at the current density of 1 A g^{-1}, and was able to endure the high discharge rate at the current density of 40 A g^{-1}.[227] α-$Ni(OH)_2$ nanosheets could be vertically grown on surface of individual CNTs in CNT paper to form hierarchical nanowires by chemical bath deposition.[228] This novel structure had an electrochemical capacitance high to 1144 F g^{-1} at the current density of 0.5 A g^{-1}, and maintained 585 F g^{-1} at 10 A g^{-1}. Flexible α-$Ni(OH)_2$ nanofibers could also be intertwined and wrapped homogenously on polypyrrole-based carbon networks, leading to formation of complex networks.

A specific capacitance of 1745 F g^{-1} could be obtained for $Ni(OH)_2$/CNT composite at 30 mA cm^{-2}.[229] Uniform and conformal coating of α-Ni(OH) flakes on carbon microfibers was deposited *in situ* by chemical bath method at room temperature. The microfibers coated α-Ni(OH) flakes exhibited five times higher in specific capacitance compared to non-conformal flakes, and the improvement was scribed to 3D network of the fibrous carbon fabric.[230]

Recently, graphene based composites have been performed by incorporating guest materials into 2D graphene sheets for improving their performance.[231-232] rGO/CNTs/α-$Ni(OH)_2$ composites were synthesized by a one-pot hydrothermal route. Their electrochemical capacitance depends on the amount of CNTs to a large extent and the composite with optimized ratio exhibited the high specific capacitance of 1320 F g^{-1} at 6 A g^{-1}.[233] Reduce GO/CNT formed a 3D conductive network in the composite which promoted not only efficient charge transport and facilitated the electrolyte diffusion, but also prevented effectively the volume expansion/contraction and aggregation of α-$Ni(OH)_2$ during charge/discharge process.[233] Low defect density graphene-supported $Ni(OH)_2$ sheets fabricated *via* hydrothermal method was reported by Zhu *et al*,[234] where graphene simultaneously acts as both nucleation center and template for the *in situ* growth of smooth and large scale $Ni(OH)_2$ nanosheets. The specific capacitance of the as-obtained composite is 1162.7 F g^{-1} at a scan rate of 5 mV s^{-1} and 1087.9 F g^{-1} at a current density of 1.5 A g^{-1}. Meanwhile, there was no marked decrease in capacitance at a current density of 10 A/g after 2,000 cycles.[234] 3D porous graphene hollow sphere frameworks were fabricated by integrating GO with amino-modified SiO_2 nanoparticles followed by etching and were used as a support to combine with α-$Ni(OH)_2$ nanoparticles, as exhibited in **Fig. 20**. These porous graphene hollow spheres had formed a continuous framework and there was a homogeneous coating of $Ni(OH)_2$ throughout the 3D framework. The $Ni(OH)_2$ exhibited a specific capacitance of 2815 F g^{-1} at 5mV s^{-1}. Increasing the scan rate to 200mV s^{-1}, α-$Ni(OH)_2$ still maintained a specific capacitance of 1950 F g^{-1} with a capacitance retention of about 70%.[235]

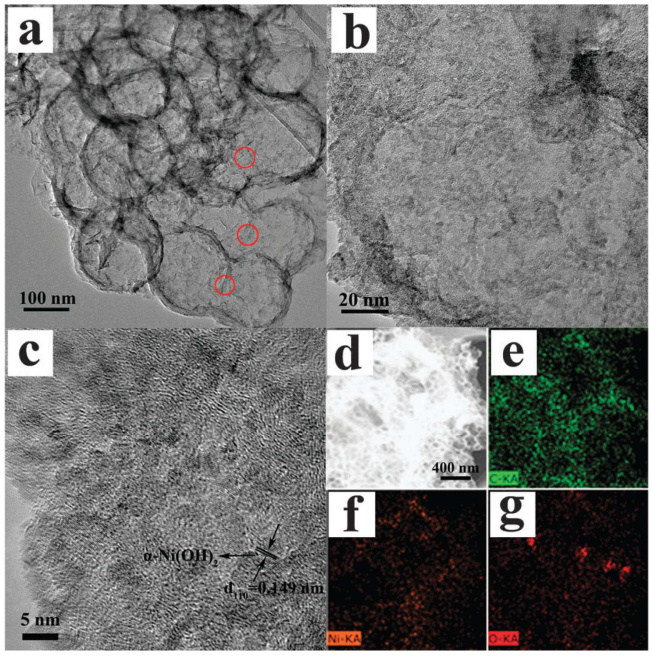

Fig. 20 (a-c) TEM images at different magnifications and (d-g) STEM-mapping of porous graphene hollow spheres combined with α-$Ni(OH)_2$. Reproduced from Ref. 235 with permission from the PCCP Owner Societies.

In addition to above carbon materials, ZnO is also a conductive candidate substrate for α-$Ni(OH)_2$ crystals to anchor in order to make a binder-free electrode for ECs.[236] Fan *et al.* employed ZnO nanowire electrode as a 3D framework to support large-area α-$Ni(OH)_2$ growth and utilized the ZnO nanowires with a good electrical conductivity to provide a natural pathway for electron transport, as shown in **Fig. 21**.[237] As each individual flake was connected to ZnO nanowire, the need for binders or conducting additives, which added extra contact resistance or weight, was eliminated. However, the possible corrosion in basic solution of ZnO might be one drawback after long cycling time.

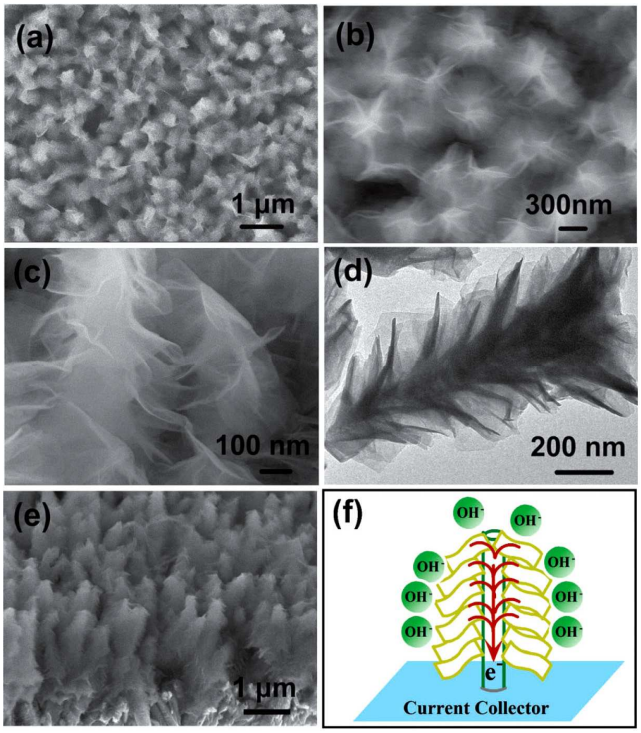

Fig. 21 (a-c) General SEM images, (d) TEM image and (c) cross-sectional SEM images of the Ni hydroxide-ZnO hybrid structure, (f) schematic diagram showing the kinetic advantage of the hybrid array in electrochemical energy storage. Taken from Ref. 237 with permission from RSC Publications.

5. Fe-based hydroxides

Comparing with nickel and cobalt, iron is much cheaper and more abundant in the earth. Fe-based oxide and hydroxides (FeOOH) have recently also attracted great interests due to their natural abundance and eco-friendliness as electrodes of lithium ion battery and supercapacitors, in addition to as catalyst, adsorbent and magnetic material.[238]

Cheng *et al.* first confirmed that FeOOH was suitable for using it as a negative electrode for hybrid ECs with an activated carbon positive electrode. The hybrid EC exhibited an estimated specific energy of 45 Wh kg^{-1} based on the total weight of two electrodes with a good cycling performance, remaining 96% initial capacity after 800 cycles.[239] Similarly, Jin also reported that the hybrid EC containing nano-sized columned FeOOH negative electrode and MnO_2 positive electrode demonstrated an energy density of 12 Wh kg^{-1} and a power density of 3700 W kg^{-1}.[240]

Various morphologies of FeOOH materials have been fabricated and used as electrode

materials of ECs.[241-243] Marygold-like structured nickel doped (5 at.%) iron hydroxide thin film was deposited on stainless steel using electrodeposition and used for ECs application. The highest specific capacitance was 287 F g^{-1} in 1 M Na_2SO_3 electrolyte at the scan rate of 10 mV s^{-1}.[244] Large area self-standing γ-FeOOH nanosheets fabricated on iron foil were evaluated as electrode of ECs in various electrolytes. It exhibited an areal capacitance of 0.3-0.4 F cm^{-2} and good cycling stability in Na_2SO_3 electrolyte, while, it was not stable in Na_2SO_4 solution.[245]

The fabrication of the composite containing FeOOH and rGO was recently developed in order to obtaine a high-performance electrode with good rate-capability and stability.[246] FeOOH nanorod/rGO composites prepared by solution method had a high electrochemical capacitance of 165.5 F g^{-1} with an excellent recycling capability.[247] Urea was employed to reduce and dope GO to N-doped graphene, and simultaneously hydrolyzed to fabricate metal hydroxide. FeOOH nanorods could be thus randomly dispersed on N-doped graphene sheets. The specific capacitance of N-doped graphene/FeOOH nanorods was improved to be 309 F g^{-1}.[248]

6. Other transition metal hydroxides

Beside Ni-, Co-, Fe- based hydroxide, other transition metal hydroxides including $Mn(OH)_2$, $Cu(OH)_2$, and $Cd(OH)_2$ were also reported as electrode materials of ECs.

Octahedral $Mn(OH)_2$ nanoparticles with a size range from 140 to 200 nm had been fabricated by a sonochemial irradiation method for the energy storage applications. It exhibited a specific capacitance of 127 F g^{-1} at a current density of 0.5 mA cm^{-2} in the potential range from -0.1 to 0.8 V in 1 M Na_2SO_4 solution.[249] Using spray coating, $Mn(OH)_2$/multi-walled CNT composite thin films could be prepared on flexible indium tin oxide/polyethylene terephthalate substrate. The capacitance increased with the weight ratio of $KMnO_4$/CNTs up to 1.6. The highest specific capacitance obtained at a scan rate of 20 mV s^{-1} was 297.5 F g^{-1} for the composite thin film with the weight ratio of $KMnO_4$/CNTs of 1.2.[250]

Copper hydroxide thin films on glass and stainless steel substrates were prepared by soft chemical synthesis route at room temperature. The room temperature chemical synthesis route allowed to form the nanograined and hydrophilic $Cu(OH)_2$ thin films. It exhibited a specific capacitance of 120 F g^{-1} in 1 M NaOH solution.[251]

A conductive additive-free and binder-less $Cd(OH)_2$ nanowires electrode were prepared via the direct growth of $Cd(OH)_2$ nanowires onto nickel foam current collector *via* a simple solution growth method. The as-prepared $Cd(OH)_2$ nanowires electrode showed an excellent pseudocapacitive performance with a specific capacitance of 1164.8 F g^{-1} at 1 A g^{-1} in 6 M KOH solution. However, the precursor solutions were harmful to the environment.[252]

The hydroxide decorated graphene composites displayed better performance over pure $MnSn(OH)_6$ nanoparticles because the graphene sheets acted as conductive bridges improving the ionic and electronic transport. The total specific capacitance depended strongly on the crystallinity of the $MnSn(OH)_6$ nanoparticles, where the materials with a poor crystallinity showed the maximum specific capacitance of 31.2 F g^{-1} (59.4 F g^{-1} based on the mass of $MnSn(OH)_6$ nanoparticles) at the scan rate of 5 mV s^{-1}.[253]

7. Hierarchical composite materials containing metal hydroxides

Up to now, porous carbon materials, transition-metal oxides or hydroxides are promising candidates for the electrode materials of ECs, but each kind of these materials has its own

advantages and disadvantages. To achieve a breakthrough in energy-storage and energy-conversion devices for capacitors, facile fabrication of the multiphase composite as electrodes is crucial, because these components enhance reaction kinetics and reduce cost. In this section, hierarchically porous heterostructure composites containing metal hydroxides as the electrode material of ECs are reviewed briefly in this section.

For electrode materials of ECs, the ion transfer and electron conduction are two main factors that determine their electrochemical performances. The hybrid nanostructured electrodes with a high specific surface area and porous configuration can lead to a large electrode/electrolyte contact area, short the diffusion path to current carriers, and high electron conductivity in electrodes.[254-255] Huang *et al.* fabricated and tested the electrochemical performance of supercapacitor electrodes consisting of $Ni(OH)_2$ nanosheets coated on $NiCo_2O_4$ nanosheets grown on carbon fiber paper current collectors. When the $NiCo_2O_4$ nanosheets were replaced by Co_3O_4 nanosheets, however, the energy and power density as well as the rate capability of the electrodes were significantly reduced, due to the lower conductivity of Co_3O_4 than that of $NiCo_2O_4$.[256] Similar work has also been carried out by Xu *et al.*,[257] where $NiCo_2O_4$@$Co_xNi_{1-x}(OH)_2$ core–shell nanosheet arrays on Ni foam had the maximum areal capacitance of 887.5 mF cm^{-2}. The $Co_3O_4/Ni(OH)_2$ composite mesoporous nanosheet networks were synthesized on a conductive substrate for supercapacitor application by heat treatment of $Co(OH)_2/Ni(OH)_2$. The resulting products also had been directly employed as EC electrodes, and they exhibited predominant electrochemical performances, such as a high specific capacitance value of 1144 F g^{-1} at 5 mV s^{-1} and long-term cyclability.[258]

The core-shell nanostructures have shown promise in these systems recently, owing to the synergistic effects of the individual components, where the core materials generally have a high electron conductivity and the shells are porous oxides or hydroxides. A hybrid nanostructure of porous cobalt monoxide nanowire@ultrathin $Ni(OH)_2$ nanoflake core-shell was directly synthesized on nickel foam by a two-step hydrothermal route, which demonstrated a specific capacitance of 798.3 F g^{-1} at the current density of 1.67 A g^{-1} and good rate performance as electrode material for supercapacitors, as reported by Guan.[259] Nanoarchitectured fibrous Co_3O_4@$Ni(OH)_2$ core−shell material grown on a nickel foam collector with excellent pseudocapacitive behaviors was fabricated by combining hydrothermal synthesis and chemical-bath deposition methods. By combining the Co_3O_4@$Ni(OH)_2$-based electrode with reduced GO or active carbon, a series of Co_3O_4@$Ni(OH)_2$-based asymmetric ECs prototypes could be developed. These asymmetric ECs exhibited superior performance, such as high specific capacitance and high energy density. Because of the large mass loading and high energy density, the prototype could drive a minifan or light a bulb even though its size was very small,[260] as shown in **Fig. 22**. $Co(OH)_2$ and $Mn(OH)_2$ nanosheets could also be electrochemically deposited on the Co_3O_4 core nanowires to form core/shell arrays. The $Co_3O_4/Co(OH)_2$ core/shell nanowire arrays were evaluated as a supercapacitor cathode material that exhibited high specific capacitances of 1095 F g^{-1} at 1 A g^{-1} and 812 F g^{-1} at 40 A g^{-1}, respectively.[261] Co_3O_4@NiAl-LDH core/shell nanowire arrays with hierarchical structure had been synthesized by *in situ* growth of LDH nanosheets shell on the surface of Co_3O_4 nanowire arrays, as reported by Duan group.[262] This structure exhibited promising supercapacitance performance with largely enhanced specific capacitance and rate capability, much superior to pristine Co_3O_4 nanowire arrays due to its hierarchically mesoporous morphology and the strong core-shell binding interaction.

In addition to these high conductive metal oxides as the core of metal hydroxide, TiN nanowires were also applied as supports of $Ni(OH)_2$, because TiN had great promise as electrode material owing to its desirable electrical conductivity and mechanical stability.[263] TiO_2 nanorods were also selected as supports to combine with $Co(OH)_2$ nanowall array, thus a novel hierarchical electrode with an improved performance was obtained.[264] Even $K_2Ti_4O_9$ nanowires grown on Ti substrate were coated by $Ni(OH)_2$ nanosheets to make a core-shell heterostructure, where the heterostructure delivered a high specific capacitance in aqueous and solid-state electrolytes.[265]

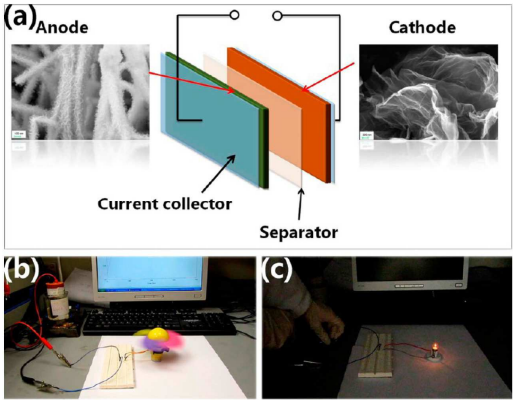

Fig. 22 (a) Schematic illustration of the fabricated Co_3O_4@$Ni(OH)_2$//RGO asymmetric supercapacitor prototype in 6 M KOH electrolyte. Photographs of the Co_3O_4@$Ni(OH)_2$//RGO asymmetric supercapacitor prototype as a power supply for a minifan (b) and a bulb (c). Reprinted with permission from Ref. 260 Copyright (2013) American Chemical Society.

Sun *et al.* designed and synthesized 3D hierarchical heterostructures of dense MnOOH nanosheets on porous hierarchical NiO nanosheet arrays, as shown in **Fig. 23**. In this configuration, porous hierarchical NiO nanosheet arrays could serve as fast ion and electron transport model, and MnOOH ultrathin nanosheets could enhance the contact surface area and assist ions penetrate into the core region to realize the release of potential electrochemical properties of NiO nanosheet arrays. These heterostructures provided intense needed critical function for efficient use of metal oxide and hydroxide in ECs. As an electrode, the 3D NiO@MnOOH core/shell nanosheet hierarchies exhibited excellent electrochemical performances, *i.e.*, high specific capacitance of 1625.3 F g^{-1} at a current density of 4 A g^{-1} with a good rate capability and high energy density (80.0 Wh kg^{-1}).[266]

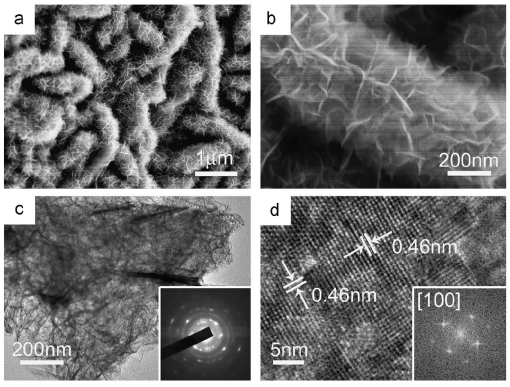

Fig. 23 (a, b) SEM images of the NiO@MnOOH core/shell nanosheet hierarchies. (c, d) TEM and HRTEM

images of the MnOOH nanosheets, two lower-right insets in (c and d) are the corresponding SAED and FFT patterns, respectively. Reprinted with permission from Ref. 266 Copyright (2014) Elsevier Ltd.

Very recently, Kang *et al.* reported an approach to fabricate low-cost transition-metal based oxy-hydroxide@nanoporous metal electrodes by electrochemical polarization of a dealloyed nanoporous Ni-Mn alloy in an alkaline solution. The hybrid electrode had a high volumetric specific capacitance (505 F cm^{-3}) and excellent rate-capacity performance.[267] His study may pave a new way to fabricate oxide-hydroxide/nanoporous metal hybrid electrodes with unprecedented properties for high-performance ECs.

8. Asymmetric supercapacitors based on metal hydroxide

According to the cell configuration for ECs, there are two kinds of ECs, symmetric and asymmetric/or hybrid ECs. Symmetric ECs are formed with two similar electrode materials as a cathode and anode, while two dissimilar electrode materials form the asymmetric ECs. The asymmetric design is an attractive approach to increasing the energy density of ECs as it can lead to an almost doubling of device capacitance. Asymmetric ECs incorporate both a polarisable and non-polarisable electrode, consisting of a polarisable electrode (usually high surface area carbon) and a battery type electrode (usually a Faradic or intercalating metal oxide).[268-270] Common symmetric EC is difficult to have a higher capacitance with higher operating voltage because of the limited potential window, while asymmetric capacitor can deliver charge with a higher operating voltage.[271] Recently, asymmetric or hybrid ECs are regarded as the new trend in supercapacitor.[272]

$Co(OH)_2$ is an importance electrode material for asymmetric supercapacitor, for there have several reports on it application in asymmetric ECs.[273-274] Asymmetric capacitor CNT-α-$Co(OH)_2$ was prepared with a low electrode resistance of 0.42 Ωcm^2. Although α-$Co(OH)_2$ raises the electrode resistance, it can enhances the cell energy capacity greatly to be 7.8 Wh kg^{-1}.[275] Cheng *et al.* fabricated graphene–CNT and graphene–CNT–$Co(OH)_2$ electrodes and assembled them in asymmetric ECs. Single-walled CNTs could act as a conductive spacer as well as a conductive binder in the composite. A high energy density of 172 Wh kg^{-1} and a maximum power density of 198 kW kg^{-1} were obtained in ionic liquid electrolyte EMI-TFSI.[276]

Nickel hydroxide or its composites are also popularly used as positive electrode of asymmetric ECs with a high specific capacitance and a high energy density,[277] typically for these hydroxides films anchored on a current collector directly.[278-281] The asymmetric EC with the highest power density of 44 Wh kg^{-1} was made using porous β-$Ni(OH)_2$ films deposited on lightweight and highly conductive surface ultrathin-graphite foam as the positive electrode, microwave exfoliated GO as negative electrode, as shown in **Fig. 24**. After 10,000 cycles, 63.2% capacitance could be remained. Its highest power density is comparable to or higher than high-end commercially available supercapacitor.[279] The asymmetric EC consisting $Ni(OH)_2$/CNTs directed grown on Ni foam positive electrode and active carbon negative electrode could deliver cell voltage of 1.8 V and an energy density of 50.6 Wh kg^{-1}, about 10 times higher than that of traditional electrochemical double layer capacitor, as reported by Gao.[280] The graphene-supported $Ni(OH)_2$-nanowires and CMK-5 were used as the positive and negative electrode, respectively, to form a high performance hybrid supercapacitor which could deliver a maximum specific power density of 40840 W kg^{-1} with a high energy density of about 17.3 Wh kg^{-1}.[282] Yan *et al.*

assembled an asymmetric EC using α-$Ni(OH)_2$/graphene and porous graphene as the positive and negative electrodes, respectively. The asymmetrical EC showed a high specific capacitance of 218.4 F g^{-1}, high energy density (77.8 Wh kg^{-1}), and good cycling stability at an operating voltage of about 1.6 V in KOH aqueous electrolytes.[283] Wang *et al.* compared the asymmetric ECs made of $Ni(OH)_2$/graphene with RuO_2/graphene. The ECs made of $Ni(OH)_2$/graphene and RuO_2/graphene showed a high specific capacitance and a high energy density with a 1.5 V operating voltage.[284]

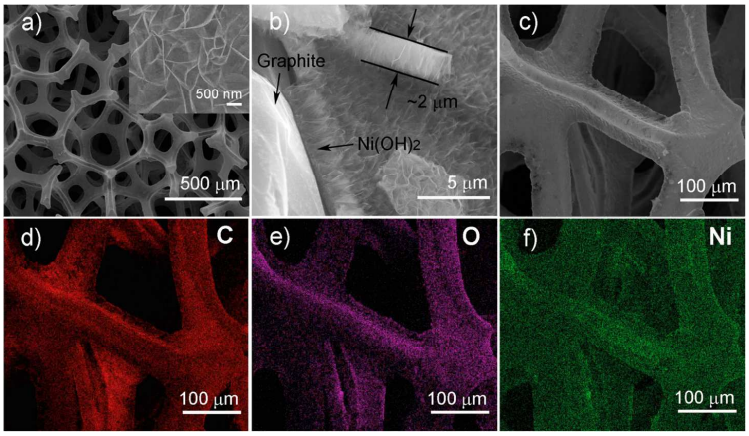

Fig. 24 SEM images of the $Ni(OH)_2$/ultrathin graphite foam composite, (a) SEM image of the composite material, and the inset shows a higher magnification image of the $Ni(OH)_2$ nanoflakes; (b) a cross-sectional view of the composite; (c) SEM image and the corresponding EDS elemental mapping images of (d) carbon, (e) oxygen, and (f) nickel. Reprinted with permission from Ref. 279 Copyright (2013) American Chemical Society.

Guest metal doping or substitution in $Ni(OH)_2$ was reported to improve the electrode materials of asymmetric ECs. Kong group reported that Al-substitution could make a stabilized α-$Ni(OH)_2$ and 7.5% Al containing α-$Ni(OH)_2$ exhibited a specific capacitance of 127 F g^{-1} and energy density of 42 Wh kg^{-1}.[285] Their XRD results proved that the addition of Al over 7.5% leaded to a higher crystallinity and increased the structure stability in alkaline medium. $Ni(OH)_2$ prepared by co-precipitation with Zn and Co as positive electrode material of an asymmetric EC both exhibited a higher specific capacitance than pure $Ni(OH)_2$.[286] The improved properties were attributed to co-precipitated Zn and Co, because the formed $Zn(OH)_2$ with $Ni(OH)_2$ could inhabit the formation of γ-NiOOH and the distributed cobalt in the lattice or on the surface of $Ni(OH)_2$ could maintain a good conductivity.[286]

Meanwhile, some LDHs such as NiAl-,[287] CoAl-,[288] and CoNi- [287,289-293] LDHs or their composites, and $Ni(OH)_2$ [56, 294-296] have also been fabricated as electrode of asymmetric supercapacitors. They all showed greatly potential energy storage ability and high rate capability.

9. Conclusion and prospective

These earth abundant metal hydroxides as electrode material are very suitable for the development of ECs. These low-cost and high-performance active hydroxide materials realized by simple and scalable solution process can offer great promise in developing novel materials for energy storage device in the future. An effective route is using 3D porously hierarchical hydroxides. These 3D pseudocapacitor electrodes have a number of features, such as fast ion and electron transfer, easy access of pseudoactive species and efficient utilization and excellent

reversibility. Though 3D nanoporous architectures have been shown to have advantages in supercapacitor, designing and fabrication of high performance electrode materials having 3D hierarchical structures with large specific area and excellent rate capability still remains a challenge.

Although most transition metal hydroxides, such as $Co(OH)_2$, $Ni(OH)_2$, and CoAl-, NiAl-LDHs are promising electrode materials for electrochemical capacitors on account of their high theoretical specific capacitance and low cost, its application is still been hindered by their low measured specific capacitance and poor cycle stability that are often associated with low specific surface area and poor electrical conductivity. Thus, two methods are usually applied to overcome this problem. One method is combining a metal hydroxide into a composite with an electronically conductive material such as carbon nanotube, graphene (reduced GO), active carbon, *etc*. The conductive material acts as both support and electron collector, while the hydroxide plays the role of electrochemically active species to form a synergistic effect. The composite consisting of metal hydroxides and carbon materials is rather promising for ECs application. The other method is direct fabricating metal hydroxide crystal films onto a current collector. These films of transition metal hydroxides deposited on conductive substrates can be used as EC electrodes straightforward. In this case, any polymer binders and conducting agents are not necessary to be applied, thus resulting in a high specific capacitance and good rate capability. Therefore, various approaches have been employed to prepare nanostructure films of metal hydroxides on conductive substrates directly, typically for hydrothermal and electrochemical deposition. However, these two methods have some intrinsic shortcomings. Hydrothermal method is limited by its volume size, incontinuous procedure and long reaction time. Electrochemical deposition technique is suffering from the disadvantages like small area of deposition, extreme cleaning after each deposition, and high working cost. Moreover, the mass loading of active materials on the substrate is usually low and hard to be precisely controlled. Thus, these issues limit the application of hydroxide films as electrode in a large scale.

For practical application, cyclic stability is crucial for an electrode material in electrochemical capacitors. An excellent cycle performance can be attributed to a few factors. One of the most important factors is the stable structure of electrode material. The structure and phase of the electroactive materials should not change during the repeated charge-discharge cycles. Typically for these porous materials, the pore size and volume are of great significance to provide good ion diffusion in the electrolyte to electrode surface. Some reports found that the capacitance decay was even caused by the dissolution of active materials in electrolyte. A facile electron transport through electrode material to current collector should be guaranteed, facilitating electrons to the current collector to improve the electronic and ionic conductivities. Thus, a low internal resistance of the electrode is necessary. A good wettability/or accessibility between electrolyte and electrode materials is also needed. Therefore, the functional groups on electrode materials should be concerned.

It is clear to find that the structure of metal hydroxides has great influence on their electrochemical properties. Hydrotalcite-like structured hydroxides show much more potential than the hydroxide materials having a brucite structure. Owing to their tunable composition, flexible interlayer spacing, hydrotalcite-like hydroxides have been deemed as one of the most outstanding electrode materials for ECs, including α-$Co(OH)_2$ and α-$Ni(OH)_2$. However, the susceptibility of their structure in an alkaline media as electrolyte is an inevitable disadvantage.

From the theoretical viewpoint, hierarchical heterostructure composites containing metal hydroxides as shell and semiconducting metal oxide as core are promising candidates for the electrode materials of ECs. The hybrid nanostructured electrodes usually have a high specific surface area and porous configuration, leading to a large electrode/electrolyte contact area, short the diffusion path to current carriers, and high electron conductivity. However, the fabrication processes for these heterostructure composites are multi-stepped and complicated, becoming a large obstacle to its practical application in EC electrodes.

Acknowledgements

This work was financially supported by Zhejiang Provincial Natural Science foundation of China under grant No. LY13E020002, Experimental research project of Zhejiang University.

References

1 P. Simon, Y. Gogotsi, *Nat. Mater.*, 2008, **7**, 845-854.
2 X. Li, B. Q. Wei, *Nano Energy*, 2013, **2**, 159-173.
3 (a) J. R. Miller and P. Simon, *Science*, 2008, **321**, 651-652; (b) K. Wang, H. P. Wu, Y. N. Meng, Z. X. Wei, *Small*, 2014, **10**, 14-31.
4 G. P. Wang, L. Zhang, J. J. Zhang, *Chem. Soc. Rev.*, 2012, **41**, 797-828.
5 S. Faraji, F. N. Ani, *J. Power Sources*, 2014, **263**, 338-360.
6 Q. Yang, Z. Y. Lu, J. F. Liu, X. D. Lei, L. Luo, X. M. Sun, *Prog. Nat. Sci. Mater. Int.*, 2013, **23**, 351-366.
7 X. Peng, L. L. Peng, C. Z. Wu, Y. Xie, *Chem. Soc. Rev.*, 2014, **43**, 3303-3323.
8 S. Liu, S. H. Sun, X. Z. You, *Nanoscale*, 2014, **6**, 2037-2045.
9 Z. S. Wu, G. M. Zhou, L. C. Yin, W. C. Ren, F. Li, H. M. Cheng, *Nano Energy*, 2012, **1**, 107-131.
10 C. D. Lokhande, D. P. Dubal, O. S. Joo, *Curr. Appl. Phys.*, 2011, **11**, 255-270.
11 W. T. Deng, X. B. Ji, Q. Y. Chen, C. E. Banks, *RSC Adv.*, 2011, **1**, 1171-1178.
12 W. F. Wei, X. W. Cui, W. X. Chen, D. G. Ivey, *Chem. Soc. Rev.*, 2011, **40**, 1697-1721.
13 C. J. Xu, F. Y. Kang, B. H. Li, H. D. Du, *J. Mater. Res.*, 2010, **25**, 1421-1432.
14 M. Aghazadeh, S. Dalvand, M. Hosseinifard, *Ceram. Int.*, 2014, **40**, 3485-3493.
15 X. H. Liu, B. H. Qu, F. H. Zhu, L. Y. Gong, L. H. Su, L. Q. Zhu, *J. Alloys Compd.*, 2013, **560**, 15-19.
16 M. Aghazadeh, H. M. Shiri, A. A. M. Barmi, *Appl. Surf. Sci.*, 2013, **273**, 237-242.
17 (a) L. Cao, F. Xu, Y. Y. Liang, H. L. Li, *Adv. Mater.* 2014, **16**, 1853-1857; (b) Z. A. Hu, L. P. Mo, X. J. Feng, J. Shi, Y. X. Wang, Y. L. Xie, *Mater. Chem. Phys.*, 2009, **114**, 53-57.
18 J. P. Cheng, M. Li, W. F. Zhang, J. S. Wu, F. Liu, X. B. Zhang, *RSC Adv.*, 2013, **3**, 13304-13310.
19 L. Y. Gong, L. H. Su, *Appl. Surf. Sci.*, 2011, **257**, 10201-10205.
20 X. B. Ji, P. M. Hallam, S. M. Houssein, R. Kadara, L. M. Lang, C. E. Banks, *RSC Adv.*, 2012, **2**, 1508-1515.
21 Y. F. Tang, Y. Y. Liu, S. X. Yu, S. C. Mu, S. H. Xiao, Y. F. Zhao, F. M. Gao, *J. Power Sources*, 2014, **256**, 160-169.
22 M. Aghazadeh, S. Dalvand, *J. Electrochem. Soc.*, 2014, **161**, 18-25.
23 S. C. Tang, S. Vongehr, Y. Wang, L. Chen, X. K. Meng, *J. Solid State Chem.*, 2010, **183**, 2166-2173.
24 J. P. Cheng, X. Chen, J. S. Wu, F. Liu, X. B. Zhang, V. P. Dravid, *CrystEngComm*, 2012, **14**, 6702-6709.
25 X. Chen, J. P. Cheng, Q. L. Shou, F. Liu, X. B. Zhang, *CrystEngComm*, 2012, **14**, 1271-1276.
26 L. B. Kong, J. J. Cai, L. L. Sun, J. Zhang, Y. C. Luo, L. Kong, *Mater. Chem. Phys.*, 2010, **122**, 368-373.
27 C. Mondal, M. Ganguly, P. K. Manna, S. M. Yusuf, T. Pal, *Langmuir*, 2013, **29**, 9179-9187.
28 C. M. Wu, C. Y. Fan, I. W. Sun, W. T. Tsai, J. K. Chang, *J. Power Sources*, 2011, **196**, 7828-7834.

29 J. K. Chang, C. M. Wu, I. W. Sun, *J. Mater. Chem*., 2010, **20**, 3729-3735.

30 Men and C. Yan, *J. Inorg. Mater.*, 2013, **28**, 1321-1327.

31 X. M. Ni, H. G. Zheng, X. K. Xiao, X. Jin, G. X. Liao, *J. Alloys Compd.*, 2009, **484**, 467-471.

32 T. Xue, J. M. Lee, *J. Power Sources*, 2014, **245**, 194-202.

33 T. Xue, X. Wang, J. M. Lee, *J. Power Sources*, 2012, **201**, 382-386.

34 C. Z. Yuan, X. G. Zhang, L. R. Hou, L. F. Shen, D. K. Li, F. Zhang, C. G. Fan, J. M. Li, *J. Mater. Chem.*, 2010, **20**, 10809-10816.

35 X. Tian, H. Y. Gao, M. Yang, Y. Luan, W. J. Dong, Z. K. Jin, J. Yu, Y. Qi, Y. H. Feng, G. Wang, *J. Alloys Compd.*, 2014, **608**, 278-282.

36 A. D. Jagadale, V. S. Jamadade, S. N. Pusawale, C. D. Lokhande, *Electrochim. Acta*, 2012, **78**, 92-97.

37 W. J. Zhou, D. D. Zhao, M. W. Xu, C. L. Xu, H. L. Li, *Electrochim. Acta*, 2008, **53**, 7210-7219.

38 M. Li, S. H. Xu, T. Liu, F. Wang, P. X. Yang, L. W. Wang, P. K. Chu, *J. Mater. Chem. A*, 2013, **1**, 532-540.

39 W. J. Zhou, M. W. Xu, D. D. Zhao, C. L. Xu, H. L. Li, *Microporous Mesoporous Mater.*, 2009, **117**, 55-60.

40 W. J. Zhou, J. Zhang, T. Xue, D. D. Zhao, H. L. Li, *J. Mater. Chem.*, 2008, **18**, 905-910.

41 A. D. Jagadale, V. S. Kumbhar, D. S. Dhawale, C. D. Lokhande, *Electrochim. Acta*, 2013, **98**, 32-38.

42 A. A. M. Barmi, M. Aghazadeh, B. Arhami, H. M. Shiri, A. A. Fazl, E. Jangju, *Chem. Phys. Lett.*, 2012, **541**, 65-69.

43 F. Cao, G. X. Pan, P. S. Tang, H. F. Chen, *J. Power Sources*, 2012, **216**, 395-399.

44 B. G. Choi, M. H. Yang, S. C. Jung, K. G. Lee, J. G. Kim, H. S. Park, T. J. Park, S. B. Lee, Y. K. Han, Y. S. Huh, *ACS Nano*, 2013, **7**, 2453-2460.

45 Z. X. Tai, J. W. Lang, X. B. Yan, Q. J. Xue, *J. Electrochem. Soc.*, 2012, **159**, 485-491.

46 R. R. Salunkhe, B. P. Bastakoti, C. T. Hsu, N. Suzuki, J. H. Kim, S. X. Dou, C. C. Hu, Y. Yamauchi, *Chem. Eur. J.*, 2014, **20**, 3084-3088.

47 L. Wang, C. Lin, F. X. Zhang, J. Jin, *ACS Nano*, 2014, **8**, 3724-3734.

48 A. K. Mondal, D. Su, S. Q. Chen, B. Sun, K. F. Li, G. X. Wang, *RSC Adv.*, 2014, **4**, 19476-19481.

49 G. J. Shao, Y. Yao, S. P. Zhang, P. He, *Rare Metals*, 2009, **28**, 132-136.

50 J. Li, F. L. Luo, X. Q. Tian, Y. Lei, H. Y. Yuan, D. Xiao, *J. Power Sources*, 2013, **243**, 721-727.

51 J. W. Lang, L. B. Kong, W. J. Wu, M. Liu, Y. C. Luo, L. Kang, *J. Solid State Electrochem.*, 2009, **13**, 333-340.

52 Y. Tian, X. H. Zhou, L. P. Huang, M. Liu, *J. Inorg. Organomet. Polym.*, 2013, **23**, 1425-1430.

53 S. T. Xing, Q. Wang, Z. C. Ma, Y. S. Wu, Y. Z. Gao, *Ionics*, 2013, **19**, 651-656.

54 H. L. Li, S. Q. Liu, C. H. Huang, Z. Zhou,Y. H. Li, D. Fang, *Electrochim. Acta*, 2011, **58**, 89-94.

55 X. M. Ni, H. G. Zheng, X. K. Xiao, X. Jin, G. X. Liao, *J. Alloys Compd.*, 2009, **484**, 467-471.

56 Y. F. Tang, Y. Y. Liu, S. X. Yu, Y. F. Zhao, S. C. Mu, F. M. Gao, *Electrochim. Acta*, 2014, **123**, 158-166.

57 Y. Wang, S. L. Gai, C. X. Li, F. He, M. L. Zhang, Y. D. Yan, P. P. Yang, *Electrochim. Acta*, 2013, **90**, 673-681.

58 M. S. Wu, K. C. Huang, *Chem. Commun.*, 2011, **47**, 12122-12124.

59 H. J. Yan, J. Wang, S. N. Li, W. L. Yang, Z. Gao, Q. Liu, R. Gao, Z. S. Li, M. L. Zhang, L. H. Liu, *Electrochim. Acta*, 2013, **87**, 880-888.

60 Z. J. Luo, K. Wang, H. M. Li, S. Yin, Q. F. Guan, L. G. Wang, *CrystEngComm*, 2011, **13**, 7108-7113.

61 M. S. Wu, J. F. Wu, *J. Power Sources*, 2013, **240**, 397-403.

62 M. Wang, Y. H. Ni, L. Cao, D. Zhao, X. Ma, *J. Colloid Interface Sci.*, 2013, **401**, 8-13.

63 Z. Y. Lu, Z. Chang, W. Zhu, X. M. Sun, *Chem. Commun.*, 2011, **47**, 9651-9653.

64 G. W. Yang, C. L. Xu, H. L. Li, *Chem. Commun.*, 2008, 6537-6539.

65 Y. M. Wang, D. D. Zhao, Y. Q. Zhao, C. L. Xu, H. L. Li, *RSC Adv.*, 2012, **2**, 1074-1082.

66 D. S. Kong, J. M. Wang, H. B. Shao, J. Q. Zhang, C. N. Cao, *J. Alloys Compd.*, 2011, **509**, 5611-5616.

67 Y. H. Ko, S. Kim, J. S. Yu, *Mater. Lett.*, 2012, **84**, 132-135.

68 Y. F. Yuan, X. H. Xia, J. B. Wu, J. L. Yang, Y. B. Chen, S. Y. Guo, *Electrochim. Acta*, 2011, **56**, 2627-2632.

69 M. Aghazadeh, A. N. Golikand, M. Ghaemi, *Int. J. Hydrogen Energy*, 2011, **36**, 8674-8679.

70 D. P. Dubal, V. J. Fulari, C. D. Lokhande, *Microporous Mesoporous Mater.*, 2012, **151**, 511-516.

71 D. P. Dubal, S. H. Lee, W. B. Kim, *J. Mater. Sci.*, 2012, **47**, 3817-3821.

72 X. B. Zhou, D. X. Cao, J. C. Huang, K. Ye, S. N. Yang, T. Liu, X. W. Liu, J. L. Yin, G. L. Wang, *J. Electroanal. Chem.*, 2014, **720-721**, 115-120.

73 B. L. Hu, X. Y. Qin, A. M. Asiri, K. A. Alamry, *Electrochim. Acta*, 2013, **107**, 339-342.

74 S. Lv, H. Suo, J. M. Wang, Y. Wang, C. Zhao, S. X. Xing, *Colloids Surf., A: Physicochem. Eng. Aspects*, 2012, **396**, 292-298.

75 L. C. Wu, Y. J. Chen, M. L. Mao, Q. H. Li, M. Zhang, *ACS Appl. Mater. Interfaces*, 2014, **6**, 5168-5174.

76 G. S. Gund, D. P. Dubal, S. S. Shinde, C. D. Lokhande, *Ceram. Int.*, 2013, **39**, 7255-7261.

77 J. Q. Tian, Z. C. Xing, Q. X. Chu, Q. Liu, A. M. Asiri, A. H. Qusti, A. O. Al-Youbi, X. P. Sun, *CrystEngComm*, 2013, **15**, 8300-8305.

78 G. S. Gund, D. P. Dubal, S. B. Jambure, S. S. Shinde, C. D. Lokhande, *J. Mater. Chem. A*, 2013, **1**, 4793-4803.

79 (a) H. B. Li, M. H. Yu, F. X. Wang, P.Liu, Y. Liang, J. Xiao, C. X. Wang, Y. X. Tong, G. W. Yang, *Nat. Commun.*, 2013, **4**, 1894. (b) Y. Fu, J. M. Song, Y. Q. Zhu, C. B. Cao, *J. Power Sources*, 2014, **262**, 344-348

80 H. B. Li, M. H. Yu, X. H. Lu, P. Liu, Y. Liang, J. Xiao, Y. X. Tong, G. W. Yang, *ACS Appl. Mater. Interfaces*, 2014, **6**, 745-749.

81 J. Zhang, L. B. Kong, J. J. Cai, Y. C. Luo, L. Kang, *J. Solid State Electrochem.*, 2010, **14**, 2065-2075.

82 C. Y. Sun, Y. G. Zhu, T. J. Zhu, J. Xie, .G. S. Cao, X. B. Zhao, *J. Solid State Electrochem.*, 2013, **17**, 1159-1165.

83 (a) D. Ghosh, S. Giri, C. K. Das, *ACS Sustainable Chem. Eng.*, 2013, **1**, 1135-1142; (b) W. F. Zhang, F. Liu, Q. Q. Li, Q. L. Shou, J. P. Cheng, L. Zhang, B. J. Nelson, X. B. Zhang, *Phys. Chem. Chem. Phys.*, 2014, **14**, 16331-16337.

84 S. Chen, J. W. Zhu, X. Wang, *J. Phys. Chem. C*, 2010, **114**, 11829-11834.

85 Z. P. Li, J. P. Wang, L. Y. Niu, J. F. Sun, P. W. Gong, W. Hong, L. M. Ma, S. R. Yang, *J. Power Sources*, 2014, **245**, 224-231.

86 (a) Y. Wang, S. L. Gai, N. Niu, F. He, P. P. Yang, *J. Mater. Chem. A*, 2013, **1**, 9083-9091; (b) H. X. Chang, J. L. Kang, L. Y. Chen, J. Q. Wang, K. Ohmura, N. Chen, T. Fujita, H. K. Wu, M. W. Chen, *Nanoscale*, 2014, **6**, 5960-5966.

87 H. J. Yan, J. W. Bai, J. Wang, X. Y. Zhang, B. Wang, Q. Liu, L. H. Liu, *CrystEngComm*, 2013, **15**, 10007-10015.

88 D. L. Fang, Z. D. Chen, X. Liu, Z. F. Wu, C. H. Zheng, *Electrochim. Acta*, 2012, **81**, 321-329.

89 S. Chen, J. J. Duan, Y. H. Tang, S. Z. Qiao, *Chem. Eur. J.*, 2013, **19**, 7118-7124.

90 Y. Y. He, J. J. Zhang, J. W. Zhao, *Acta Phys. -Chim. Sin.*, 2014, **30**, 297-304.

91 J. F. Xie. X. Sun, N. Zhang, K. Xu, M. Zhao, Y. Xie, *Nano Energy*, 2013, **2**, 65-74.

92 S. D. Min, C. J. Zhao, G. R. Chen, X. Z. Qian, *Electrochim. Acta*, 2014, **115**, 155-164.

93 H. T. Zhang, X. Zhang, D. C. Zhang, X. Z. Sun, H. Lin, C. H. Wang, Y. W. Ma, *J. Phys. Chem. B*, 2013, **117**, 1616-1627.

94 C. H. Jiang, B. B. Zhan, C. Li, W. Huang, X. C. Dong, *RSC Adv.*,2014, **4**, 18080-18085.

95 H. L. Wang, H. S. Casalongue, Y. Y. Liang, H. J. Dai, *J. Am. Chem. Soc.*, 2010, **132**, 7472-7477.

96 Z. Wu, X. L. Huang, Z. L. Wang, J. J. Xu, H. G. Wang, X. B. Zhang, *Sci. Rep.*, 2014, **4**, 3669.

97 M. Shahid, J. L. Liu, I. Shakir, M. F. Warsi, M. Nadeem, Y. UK. Kwon, *Electrochim. Acta*, 2012, **85**, 243-247.

98 D. P. Dubal, G. S. Gund, C. D. Lokhande, R. Holze, *ACS Appl. Mater. Interfaces*, 2013, **5**, 2446-2454.

99 H. Chai, X. Chen, D. Z. Jia, W. Y. Zhou, *Rare Met.*, 2011, **30**, 85-89.

100 J. Zhang, L. B. Kong, J. J. Cai, H. Li, Y. C. Luo, L. Kang, *Microporous Mesoporous Mater.*, 2010, **132**, 154-162.

101 L. L. Zhang, Z. G. Xiong, X. S. Zhao, *J. Power Sources*, 2013, **222**, 326-332.

102 Z. P. Sun, X. M. Lu, *Ind. Eng. Chem. Res.*, 2012, **51**, 9973-9979.

103 J. Han, K. C. Roh, M. R. Jo, Y. M. Kang, *Chem. Commun.*, 2013, **49**, 7067-7069.

104 H. Chen, L. F. Hu, M. Chen, Y. Yan, L. M. Wu, *Adv. Funct. Mater.*, 2014, **24**, 934-942.

105 H. Chen, L. F. Hu, Y. Yan, R. C. Che, M. Chen, L. M. Wu, *Adv. Energy Mater.*, 2013, **3**, 1636-1646.

106 X. H. Liu, R. Z. Ma, Y. Bando, T. Sasaki, *Adv. Mater.*, 2012, **24**, 2148-2153.

107 X. Wang, A. Sumboja, M. F. Lin, J. Yan, P. S. Lee, *Nanoscale*, 2012, **4**, 7266-7272.

108 N. T. H. Trang, H. V. Ngoc, N. Lingappan, D. H. Kang, *Nanoscale*, 2014, **6**, 2434-2439.

109 R. R. Salunkhe, K. Jang, S. W. Lee, H. Ahn, *RSC Adv.*, 2012, **2**, 3190-3193.

110 L. J. Xie, Z. G. Hu, C. X. Lv, G. H. Sun, J. L. Wang, Y. Q. Li, H. W. He, J. Wang, K. X. Li, *Electrochim. Acta*, 2012, **78**, 205-211.

111 Z. Jiang, Z. P. Li, Z. H. Qin, H. Y. Sun, X. L. Jiao, D. R. Chen, *Nanoscale*, 2013, **5**, 11770-11775.

112 T. Yan, H. Y. Zhu, R. Y. Li, Z. J. Li, J. K. Liu, G. L. Wang, Z. Q. Gu, *Electrochim. Acta*, 2013, **111**, 71-79.

113 T. Yan, Z. J. Li, R. Y. Li, Q. Ning, H. Kong, Y. L. Niu, J. K. Liu, *J. Mater. Chem.*, 2012, **22**, 23587-23592.

114 V. Gupta, S. Gupta, N. Miura, *J. Power Sources*, 2008, **175**, 680-685.

115 Z. A. Hu, Y. L. Xie, Y. X. Wang, H. Y. Wu, Y. Y. Yang, Z. Y. Zhang, *Electrochim. Acta*, 2009, **54**, 2737-2741.

116 S. B. Kulkarni, A. D. Jagadale, V. S. Kumbhar, R. N. Bulakhe, S. S. Joshi, C. D. Lokhande, *Int. J. Hydrogen Energy*, 2013, **38**, 4046-4053.

117 T. Yan, R. Y. Li, Z. J. Li, J. K. Liu, G. L. Wang, Z. Q. Gu, *RSC Adv.*, 2013, **3**, 19416-19422.

118 J. C. Chen, C. T. Hsu, C. C. Hu, *J. Power Sources*, 2014, **253**, 205-213.

119 J. Pu, Y. Tong, S. B. Wang, E. H. Sheng, Z. H. Wang, *J. Power Sources*, 2014, **250**, 250-256.

120 I. Shakir, M. Shahid, U. A. Rana, I. M. A. Nashef, R. Hussain, *Electrochim. Acta*, 2014, **129**, 28-32.

121 M. F. Warsi, I. Shakir, M. Shahid, M. Sarfraz, M. Nadeem, Z. A. Gilani, *Electrochim. Acta*, 2014, **135**, 513-518.

122 J. Xu, Y. Z. Dong, J. Y. Cao, B. Guo, W. C. Wang, Z. D. Chen, *Electrochim. Acta*, 2013, **114**, 76-82.

123 M. Sebastian, C. Nethravathi, M. Rajamathi, *Mater. Res. Bull.*, 2013, **48**, 2715-2719.

124 X. Sun, G. K. Wang, H. T. Sun, F. Y. Lu, M. P. Yu, J. Lian, *J. Power Sources*, 2013, **238**, 150-156.

125 G. Chen, S. S. Liaw, B. S. Li, Y. Xu, M. Dunwell, S. G. Deng, *J. Power Sources*, 2013, **251**, 338-343.

126 Y. W. Cheng, H. B. Zhang, C. V. Varanasi, J. Liu, *Energy Environ. Sci.*, 2013, **6**, 3314-3321.

127 T. Yan, R. Y. Li, Z. J. Li, *Mater. Res. Bull.*, 2014, **51**, 97-104.

128 L. Y. Zhang, C. H. Tang, X. S. Yin, H. Gong, *J. Mater. Chem. A*, 2014, **2**, 4660-4666.

129 X. M. Liu, Y. H. Zhang, X. G. Zhang, S. Y. Fu, *Electrochim. Acta*, 2004, **49**, 3137-3141.

130 P. Vialat, F. Leroux, C. T. Gueho, G. Villemure, C. Mousty, *Electrochim. Acta*, 2013, **107**, 599- 610.

131 Z. Y. Lu, W. Zhu, X. D. Lei, G. R. Williams, D. O. Hare, Z. Chang, X. M. Sun, X. Duan, *Nanoscale*, 2012, **4**,

3640-3643.

132 W. Hong, J. Q. Wang, L. Y. Niu, J. F. Sun, P. W. Gong, S. R. Yang, *J. Alloy. Compd.*, 2014, **608**, 297-303.

133 Y. Wang, W. S. Yang, C. Chen, D. G. Evans, *J. Power Sources*, 2008, **184**, 682-690.

134 L. Wang, D. Wang, X. Y. Dong, Z. J. Zhang, X. F. Pei, X. J. Chen, B. Chen, J. Jin, *Chem. Commun.*, 2011, **47**, 3556-3558.

135 X. Y. Dong, L. Wang, D. Wang, C. Li, J. Jin, *Langmuir*, 2012, **28**, 293-298.

136 M. Hu, X. D. Ji, L. X. Lei, X. W. Lu, *Electrochim. Acta*, 2013, **105**, 261-274.

137 J. P. Cheng, J. H. Fang, M. Li, W. F. Zhang, F. Liu, X. B. Zhang, *Electrochim. Acta*, 2013, **114**, 68-75.

138 J. B. Han, Y. B. Dou, J. W. Zhao, M. Wei, D. G. Evans, X. Duan, *Small*, 2013, **9**, 98-106.

139 L. J. Zhang, X. G. Zhang, L. F. Shen, B. Gao, L. Hao, X. J. Lu, F. Zhang, B. Ding, C. Z. Yuan, *J. Power Sources*, 2012, **199**, 395-401.

140 S. Huang, G. N. Zhu, C. Zhang, W. W. Tjiu, Y. Y. Xia, T. X. Liu, *ACS Appl. Mater. Interfaces*, 2012, **4**, 2242-2249.

141 J. H. Hao, W. S. Yang, Z. Zhang, B. P. Lu, X. Ke, B. L. Zhang, J. L. Tang, *J. Colloid Interface Sci.*, 2014, **426**, 131-136.

142 J. H. Fang, M. Li, Q. Q. Li, W. F. Zhang, Q. L. Shou, F. Liu, X. B. Zhang, J. P. Cheng, *Electrochim. Acta*, 2012, **85**, 248-255.

143 A. Faour, C. Mousty, V. Prevot, B. Devouard, A. D. Roy, P. Bordet, E. Elkaim, C. T. Gueho, *J. Phys. Chem. C*, 2012, **116**, 15646-15659.

144 J. Wang, Y. C. Song, Z. S. Li, J. D. Zhou, X. Y. Jing, M. L. Zhang, Z. H. Jiang, *Energy Fuels*, 2010, **24**, 6463-6467.

145 Z. Wang, X. Zhang, J. H. Wang, L. D. Zou, Z. T. Liu, Z. P. Hao, *J. Colloid Interface Sci.*, 2013, **396**, 251-257.

146 Y. C. Song, J. Wang, Z. S. Li, D. H. Guan, T. Mann, Q. Liu, M. L. Zhang, *Microporous Mesoporous Mater.*, 2012, 148, 159-165.

147 F. He, Z. B. Hu, K. Y. Liu, S. R. Zhang, H. T. Liu, S. B. Sang, *J. Power Sources*, 2014, **267**, 188-196.

148 M. F. Shao, F. Y. Ning, Y. F. Zhao, J. W. Zhao, M. Wei, D. G. Evans, X. Duan, *Chem. Mater.*, 2012, **24**, 1192-1197.

149 J. B. Wei, J. Wang, Y. C. Song, Z. S. Li, Z. Gao, T. Mann, M. L. Zhang, *J. Solid State Chem.*,2012, **196**, 175-181.

150 L. Yan, R. Y. Li, Z. J. Li, J. K. Liu, Y. J. Fang, G. L. Wang, Z. G. Gu, *Electrochim. Acta*, 2013, **95**, 146-154.

151 B.Wang, Q. Liu, Z. Y. Qian, X. F. Zhang, J. Wang, Z. S. Li, H. J. Yan, Z. Gao, F. B. Zhao, L. H. Liu, *J. Power Sources*, 2014, **246**, 747-753.

152 Yan and Lin, *Acta Chim. Sinica*, 2013, **71**, 822-828.

153 A. B. Béléké, M. Mizuhata, *J. Power Sources*, 2010, **195**, 7669-7676.

154 A. B. Béléké, E. Higuchi, H. Ionue, M. Mizuhata, *J. Power Sources*, 2013, **225**, 215-220.

155 J. Memon, J. H. Sun, D. L. Meng, W. Z. Ouyang, M. A. Memon, Y. Huang, S. K. Yan, J. X. Geng, *J. Mater. Chem. A*, 2014, **2**, 5060-5067.

156 Y. L. Niu, R. Y. Li, Y. J. Fang, J. K. Liu, *Electrochim. Acta*, 2013, **94**, 360-366.

157 M. Li, J. P. Cheng, J. H. Fang, Y. Yang, F. Liu, X. B. Zhang, *Electrochim. Acta*, 2014, **134**, 309-318.

158 Z. Gao, J. Wang, Z. S. Li, W. L. Yang, B. Wang, M. J. Hou, Y. He, Q. Liu, T. Mann, P. P. Yang, M. L. Zhang, L. H. Liu, *Chem. Mater.*, 2011, **23**, 3509-3516.

159 L. J. Zhang, J. Wang, J. J. Zhu, X. G. Zhang, K. S. Hui, K. N. Hui, *J. Mater. Chem. A*, 2013, **1**, 9046-9053.

160 J. Xu, S. L. Gai, N. Niu, P. Gao, Y. J. Chen, P. P. Yang, *J. Mater. Chem. A*, 2014, **2**, 1022-1031.

161 L. Li, R. M. Li, S. L. Gai, F. He, P. P. Yang, *J. Mater. Chem. A*, 2014, **2**, 8758-8765.

162 Y. Wimalasiri, R. Fan, X. S. Zhao, L. D. Zou, *Electrochim. Acta*, 2014, **134**, 127-135.

163 M. Hu, Z. Y. Yang, L. X. Lei, Y. M. Sun, *J. Power Sources*, 2011, **196**, 1569-1577.

164 Z. P. Xu, L. Li, C. Y. Cheng, R. G. Ding, C. H. Zhou, *Appl. Clay. Sci.*, 2013, **74**, 102-108.

165 S. Werner, V. W. H. Lau, S. Hug, V. Duppel, H. C. Schaumann, B. V. Lotsch, *Langmuir*, 2013, **29**, 9199−9207.

166 J. W. Zhao, J. L. Chen, S. M. Xu, M. F. Shao, D. P. Yan, M. Wei, D. G. Evans, X. Duan, *J. Mater. Chem. A*, 2013, **1**, 8836-8843.

167 M. F. Shao, M. Wei, D. G. Evans, X. Duan, *Chem. Commun.*, 2011, **47**, 3171-3173.

168 M. A. Woo, M. S. Song, T. W. Kim, I. Y. Kim, J. Y. Ju, Y. S. Lee, S. J. Kim, J. H. Choy, S. J. Hwang, *J. Mater. Chem.*, 2011, **21**, 4286-4292.

169 Y. H. Gu, Z. Y. Lu, Z. Chang, J. F. Liu, X. D. Lei, Y. P. Li, X. M. Sun, *J. Mater. Chem. A*, 2013, **1**, 10655-10661.

170 H. W. Park, J. S. Chae, S. M. Park, K. B. Kim, K. C. Roh, *Met. Mater. Int.*, 2013, **19**, 887-894.

171 J. W. Jiang, X. G. Zhang, L. H. Su, L. J. Zhang, F. Zhang, *Chin. J. Inorg. Chem.*, 2010, **26**, 1623-1628.

172 J. W. Zhao, J. L. Chen, S. X. Xu, M. F. Shao, Q. Zhang, F. Wei, J. Ma, M. Wei, D. G. Evans, X. Duan, *Adv. Funct. Mater.*, 2014, **24**, 2938-2946.

173 L. H. Su, C, L. Ma, T. Hou, W. J. Han, *RSC Adv.*, 2013, **3**, 19807-19811.

174 J. Yang, C. Yu, X. M. Fan, Z. Ling, J. S. Qiu, Y. Gogotsi, *J. Mater. Chem. A*, 2013, **1**, 1963-1968.

175 V. Gupta, S. Gupta, N. Miura, *J. Power Sources*, 2009, **189**, 1292-1295.

176 J. B. Wei, Z. Gao, Y. C. Song, W. L. Yang, J. Wang, Z. S. Li, T. Mann, M. L. Zhang, L. H. Liu, *Mater. Chem. Phys.*, 2013, **139**, 395-402.

177 Z. P. Liu, R. Z. Ma, M. Osada, K. Takada, T. Sasaki, *J. Am. Chem. Soc.*, 2005, **127**, 13869-13874.

178 (a) X. Liu, R. Ma, Y. Bando, T. Sasaki, *Angew. Chem. Int. Ed.*, 2010, **49**, 8253-8256. (b) L. Liu, J. P. Cheng, J. Zhang, F. Liu, X. B. Zhang, *J. Alloys Compd.*, 2014, **615**, 868-874.

179 Y. L. Chen, Z. A. Hu, Y. Q. Chang, H. W. Wang, G. R. Fu, X. Q. Jin, L. J. Xie, *Chin. J. Chem.*, 2011, **29**, 2257-2262.

180 Zan Gao, W. L. Yang, Y. X. Yan, J. Wang, J. Ma, X. M. Zhang, B. H. Xing, L. H. Liu, *Eur. J. Inorg. Chem.*, 2013, 4832-4838.

181 L. B. Kong, J. W. Lang, M. Liu, Y. C. Luo, L. Kang, *J. Power Sources*, 2009, **194**, 1194-1201.

182 T. Wu, C. Z. Yuan, *Mater. Lett.*, 2012, **85**, 161-163.

183 L. R. Hou, C. Z. Yuan, L. Yang, L. F. Shen, F. Zhang, X. G. Zhang, *CrystEngComm*, 2011, **13**, 6130-6135.

184 J. Jiang, J. P. Liu, R. M. Ding, J. H. Zhu, Y. Y. Li, A. Z. Hu, X. Li, X. T. Huang, *ACS Appl. Mater. interf.*, 2011, **1**, 99-103.

185 Z. Chen, Y. Chen, C. Zuo, S. Zhou, A. G. Xiao, A. X. Pan, *Bull. Mater. Sci.*, 2013, **36**, 239-244.

186 W. L. Yang, Z. Gao, J. Ma, J. Wang, X. M. Zhang, L. H. Liu, *Dalton Trans.*, 2013, **42**, 15706-15715.

187 L. B. Kong, M. C. Liu, J. W. Lang, M. Liu, Y. C. Luo, L. Kang, *J. Solid State Electrochem.*, 2011, **15**, 571-577.

188 V. Gupta, T. Kusahara, H. Toyama, S. Gupta, N. Miura, *Electrochem. Commun.*, 2007, **9**, 2315-2319.

189 J. Tang, D.Q. Liu, Y. X. Zheng, X. W. Li, X. H. Wang, D. Y. He, *J. Mater. Chem. A*, 2014, **2**, 2585-2591.

190 J. Zhang, X. C. Wang, J. Ma, S. Liu, X. B. Yi, *Electrochim. Acta*, 2013, **104**, 110-116.

191 C. M. Zhao, X. Wang, S. M. Wang, H. X. Wang, Y. C. Yang, W. T. Zheng, *Mater. Res. Bull.*, 2013, **48**, 3189-3195.

192 T. Zhao, H. Jiang, J. Ma, *J. Power Sources*, 2011, **196**, 860-864.

193 C. M. Zhao, X. Wang, S. M. Wang, Y. Y. Wang, Y. X. Zhao, W. T. Zheng, *Int. J. Hydrogen Energy*, 2012, **37**, 11846-11852.

194 G. X. Pan, X. Xia, F. Cao, P. S. Tang, H. F. Chen, *Electrochim. Acta*, 2012, **63**, 335-340.

195 X. Ge, C. D. Gu, X. L. Wang, J. P. Tu, *J. Phys. Chem. C*, 2014, **118**, 911-923.

196 J. M. Ko, D. Soundarajan, J. H. Park, S. D. Yang, S. W. Kim, K. M. Kim, K. H. Yu, *Curr. Appl. Phys.*, 2012, **12**, 341-345.

197 Z. A. Hu, Y. L. Xie, Y. X. Wang, L. J. Xie, G. R. Fu, X. Q. Jin, Z. Y. Zhang, Y. Y. Yang, H. Y. Wu, *J. Phys. Chem. C*, 2009, **113**, 12502-12508.

198 L. Wang, Z. H. Dong, Z. G. Wang, F. X. Zhang, J. Jin, *Adv. Funct. Mater.*, 2013, **23**, 2758-2764.

199 C. Y. Yan, H. Jiang, T. Zhao, C. Z. Li, J. Ma, P. S. Lee, *J. Mater. Chem.*, 2011, **21**, 10482-10488.

200 D. T. Dam, X. Wang, J. M. Lee, *RSC Adv.*, 2012, **2**, 10512-10518.

201 D. T. Dam, J. M. Lee, *Nano Energy*, 2013, **2**, 1186-1196.

202 B. Schneiderová, J. Demel, J. Pleštil, H. Tarábková, J. Bohuslav, K. Lang, *Dalton Trans.*, 2014, **43**, 10484-10491.

203 J. P. Cheng, L. Liu, J. Zhang, F. Liu, X. B. Zhang, *J. Electroanal. Chem.*, 2014, **722-723**, 23-31.

204 C. G. Liu, Y. S. Lee, Y. J. Kim, I. C. Song, J. H. Kim, *Synthetic. Met.*, 2009, **159**, 2009-2012.

205 X. Hu, J. L. Jiang, Z. H. Fan, Z. Y. Ling, *J. Electrochem. Soc.*, 2013, **160**, 1425-1429.

206 H. W. Park, Y. T. Ju, S. M. Park, K. C. Roh, *RSC Adv.*, 2014, **4**, 567-571.

207 M. S. Wu, K. C. Huang, *Int. J. Hydrogen Energy*, 2011, **36**, 13407-13413.

208 G. R. Fu, Z. A. Hu, L. J. Xie, X. Q. Jin, Y. X. Wang, Z. Y. Zhang, Y. Y. Yang, H. Y. Wu, *Int. J. Electrochem. Sci.*, 2009, **4**, 1052-1062.

209 M. Aghazadeh, M. Ghaemi, B. Sabour, S. Dalvand, *J. Solid State Electrochem.*, 2014, **18**, 1569-1584.

210 K. Wang, L. Zhang, *Electrochem.*, 2013, 81, 259-261.

211 Y. X. Wang, Z. A. Hu, H. Y. Wu, *Mater. Chem. Phys.*, 2011, **126**, 580-583.

212 J. Liang, B. T. Dong, S. J. Ding, C. P. Li, B. Q. Li, J. Li, G. Yang, *J. Mater. Chem. A*, 2014, **2**, 11299-11304.

213 H. M. Du, L. F. Jiao, K. Z. Cao, Y. J. Wang, H. T. Yuan, *ACS Appl. Mater. Interfaces*, 2013, **5**, 6643-6648.

214 Q. L. Xian, J. Li, *J. Inorg. Mater.*, 2010, **25**, 1268-1272.

215 S. T. Xing, Q. Wang, Z. C. Ma, Y. S. Wu, Y. Z. Gao, *Mater. Lett.*, 2012, **78**, 99-101.

216 H. Jiang, T. Zhao, C. Z. Li, J. Ma, *J. Mater. Chem.*, 2011, **21**, 3818-3823.

217 D. Ghosh, S. Giri, M. Mandal, C. K. Das, *RSC Adv.*, 2014, **4**, 26094-26101.

218 X. Q. Tian, C. M. Cheng, L. Qian, B. Z. Zheng, H. Y. Yuan, S. P. Xie, D. Xiao, M. M. F. Choi, *J. Mater. Chem.*, 2012, **22**, 8029-8035.

219 Y. Ren, L. Gao, *J. Am. Ceram. Soc.*, 2010, **93**, 3560-3564.

220 B. P. Bastakoti, H. S. Huang, L. C. Chen, K. C. W. Wu, Y. Yamauchi, *Chem. Commun.*, 2012, **48**, 9150-9152.

221 G. Q. Yang, Y. Q. Wu, B. L. Wang, W. Y. Guo, Z. Y. Ren, Z. H. Bu, C. C. Miao, H. L. Li, *J. Solid State Electrochem.*, 2012, **16**, 3761-3767.

222 J. C. Huang, T. Lei, X. P. Wei, X. W. Liu, T. Liu, D. X. Cao, J. L. Yin, G. L. Wang, *J. Power Sources*, 2013, **232**, 370-375.

223 Z. You, K. Shen, Z. C. Wu, X. F. Wang, X. H. Kong, *Appl. Surf. Sci.*, 2012, **258**, 8117-8123.

224 B. K. Kim, V. Chabot, A. P. Yu, *Electrochim. Acta*, 2013, **109**, 370-380.

225 H. Fang, S. C. Zhang, T. Jiang, R. X. Lin, Y. Lin, *Electrochim. Acta*, 2014, **125**, 427-434.

226 H. L. Cheng, A. D. Su, S. H. Li, S. T. Nguyen, L. Lu, C. Y. H. Lim, H. M. Duong, *Chem. Phys. Lett.*, 2014, **601**, 168-173.

227 J. T. Zhang, S. Liu, G. L. Pan, G. R. Li, X. P. Gao, *J. Mater. Chem. A*, 2014, **2**, 1524-1529.

228 L. N. Wang, H. Y. Chen, F. Cai, M. H. Chen, *Mater. Lett.*, 2014, **115**, 168-171.

229 J. Z. Fan, H. Y. Mi, Y. L. Xu, B. Gao, *Mater. Res. Bull.*, 2013, **48**, 1342-1345.

230 N. A. Alhebshi, R. B. Rakhi, H. N. Alshareef, *J. Mater. Chem. A*, 2013, **1**, 14897-14903.

231 J. W. Xiao, S. Yang, *ChemPlusChem*, 2012, **77**, 807-816.

232 L. Q. Wang, X. C. Li, T. M. Guo, X. B. Yan, B. K. Tay, *Int. J. Hydrogen Energy*, 2014, **39**, 7876-7884.

233 X. A. Chen, X. H. Chen, F. Q. Zhang, Z. Yang, S. M. Huang, *J. Power Sources*, 2013, **243**, 555-561.

234 J. W. Zhu, S. Chen, H. Zhou, X. Wang, *Nano Res.*, 2012, **5**, 11-19.

235 F. Q. Zhang, D. Zhu, X. A. Chen, X. Xu, Z. Yang, C. Zou, K. Q. Yang, S. M. Huang, *Phys. Chem. Chem. Phys.*, 2014, **16**, 4186-4192.

236 Z. H. Pu, Q. Liu, A. H. Qusti, A. M. Asiri, A. O. Al-Youbi, X. P. Sun, *Electrochim. Acta*, 2013, **109**, 252-255.

237 J. P. Liu, C. W. Cheng, W. W. Zhou, H. X. Li, H. J. Fan, *Chem. Commun.*, 2011, **47**, 3436-3438.

238 Q. Qu, S. Yang, X. Feng, *Adv. Mater.*, 2011, **23**, 5574-5580.

239 L. Cheng, H. Q. Li, Y. Y. Xia, *J. Solid State Electrochem.*, 2006, **10**, 405-410.

240 W. H. Jin, G. T. Cao, J. Y. Sun, *J. Power Sources*, 2008, **175**, 686-691.

241 R. Barik, B. K. Jena, A. Dash, M. Mohapatra, *RSC Adv.*, 2014, **4**, 18827-18834.

242 K. F. Chen, Y. D. Noh, W. Y. Huang, J. F. Ma, S. Komarneni, *Ceram. Int.*, 2014, **40**, 2877-2884.

243 Z. C. Li, M. Y. Guan, Z. S. Lou, T. M. Shang, *Micro Nano Lett.*, 2012, **7**, 33-36.

244 V. S. Jamadade, V. J. Fulari, C. D. Lokhande, *J. Alloy. Compd.*, 2011, **509**, 6257-6261.

245 K. K. Lee, R. W. Y. Ng, K. K. She, W. S. Chin, C. H. Sow, *Mater. Lett.*, 2014, **118**, 150-153.

246 H. Xu, Z. A. Hu, A. L. Lu, L. Li, Y. Y. Yang, Z. Y. Zhang, H. Y. Wu, *Mater. Chem. Phys.*, 2013, **141**, 310-317.

247 Q. L. Shou, J. P. Cheng, L. Zhang, B. J. Nelson, X. B. Zhang, *J. Solid State Chem.*, 2012, 185, 191-197.

248 X. F. Xia, W. Lei, Q. L. Hao, W. J. Wang, Y. X. Sun, X. Wang, *Electrochim. Acta*, 2013, **113**, 117-126.

249 S. Anandan, B. G. S. Raj, G. J. Lee, J. J. Wu, *Mater. Res. Bull.*, 2013, **48**, 3357-3361.

250 J. S. Liu, Y. Hu, T. L. Chuang, C. L. Huang, *Thin Solid Films*, 2013, **544**, 186-190.

251 K. V. Gurav, U. M. Patil, S. W. Shin, G. L. Agawane, M. P. Suryawanshi, S. M. Pawar, P. S. Patil, C. D. Lokhande, J. H. Kim, *J. Alloys Compd.*, 2013, **573**, 27-31.

252 J. C. Huang, T. Liu, X. W. Liu, L. F. Du, D. X. Cao, J. L. Yin, G. L. Wang, *J. Electroanal. Chem.*, 2013, **696**, 15-19.

253 G. K. Wang, X. Sun, F. Y. Lu, Q. K. Yu, C. S. Liu, J. Lian, *J. Solid State Chem*., 2012, **185**, 172-179.

254 (a)X. F. Gong, J. P. Cheng, F. Liu, L. Zhang, X. B. Zhang, *J. Power Sources*, 2014, **267**, 610-616; (b) B. B. Wang, X. X. Fu, F. Liu, S. L. Shi, J. P. Cheng, X. B. Zhang, *J. Alloys Compd.*, 2014, **587**, 82-89.

255 (a) H. Chen, S. X. Zhou, L. M. Wu, *ACS Appl. Mater. Interfaces*, 2014, **6**, 8621-8630; (b) J. P. Cheng, B. B. Wang, M. G. Zhao, F. Liu, X. B. Zhang, *Sens. Actuators B*, 2014, **190**, 78-85.

256 L. Huang, D. C. Chen, Y. Ding, Z. L. Wang, Z. Z. Zeng, M. L. Liu, *ACS Appl. Mater. Interfaces*, 2013, **5**, 11159-11162.

257 K. B. Xu, R. J. Zou, W. Y. Li, Q. Liu, X. J. Liu, L. An, J. Q. Hu, J. Mater. Chem. A, 2014, **2**, 10090-10097.

258 J. H. Zhong, A. L. Wang, G. R. Li, J. W. Wang, Y. N. Ou, Y. X. Tong, *J. Mater. Chem.*, 2012, **22**, 5656-5665.

259 C. Guan, J. P. Liu, C. W. Cheng, H. X. Li, X. L. Li, W. W. Zhou, H. Zhang, H. J. Fan, *Energy Environ. Sci.*, 2011, **4**, 4496-4499.

260 C. H. Tang, X. S. Yin, H. Gong, *ACS Appl. Mater. Interfaces*, 2013, **5**, 10574-10582.

261 X. H. Xia, J. P. Tu, Y. Q. Zhang, J. Chen, X. L. Wang, C. D. Gu, C. Guan, J. S. Luo, H. J. Fan, *Chem. Mater.*, 2012, **24**, 3793-3799.

262 F. Y. Ning, M. F. Shao, C. L. Zhang, S. M. Xu, M. Wei, X. Duan, *Nano Energy*, 2014, **7**, 134-142.

263 H. Yi, X. Chen, H. W. Wang, X. F. Wang, *Electrochim. Acta*, 2014, **116**, 372-378.

264 A. Ramadoss, S. J. Kim, *Electrochim. Acta*, 2014, **136**, 105-111.

265 W. J. Zhou, X. J. Liu, Y. H. Sang, Z. H. Zhao, K. Zhou, H. Liu, S. W. Chen, *ACS Appl. Mater. Interfaces*, 2014, **6**, 4578-4586.

266 J. Q. Sun, W. Y. Li, B. J. Zhang, G. Li, L. Jiang, Z. G. Chen, R. J. Zou, J. Q. Hu, *Nano Energy*, 2014, **4**, 56-64.

267 J. L. Kang, A. Hirata, H. J. Qiu, L. Y. Chen, X. B. Ge, T. Fujita, M. W. Chen, *Adv. Mater.*, 2014, **26**, 269-272.

268 G. Yu, X. Xie, L. Pan, Z. Bao, Y. Cui, *Nano Energy*, 2013, **2**, 213-234.

269 N. W. Duffy, W. Baldsing, A. G. Pandolfo, *Electrochim. Acta*, 2008, **54**, 535-539.

270 F. Wang, S. Xiao, Y. Hou, C. Hu, L. Liu, Y. Wu, *RSC Adv.*, 2013, **3**, 13059-13084.

271 A. B. Yuan, Q. L. Zhang, *Electrochem. Commun.*, 2006, **8**, 1173-1178.

272 Y. Y. Liang, H. L. Li, X. G. Zhang, *Mater. Sci. Eng., A* , 2008, **473**, 317-322.

273 H. B. Kong, M. Liu, J. W. Lang, Y. C. Luo, L. Kang, *J. Electrochem. Soc.*, 2009, **156**, 1000-1004.

274 F. S. Fedorov, J. Linnemann, K. Tschulik, L. Giebeler, M. Uhlemann, A. Gebert, *Electrochim. Acta*, 2013, **90**, 166-170.

275 C. H. Chen, D. S. Tsai, W. H. Chung, K. Y. Lee, Y. M. Chen, Y. S. Huang, *J. Power Sources*, 2012, **205**, 510-515.

276 C. Qian, T. Jie, S. Y. Norio, Q. L. Chang, *Sci. Technol. Adv. Mater.*, 2014, **15**, 14206-14211.

277 Y. Tian, J. W. Yan, L. P. Huang, R. Xue, L. X. Hao, B. L. Yi, *Mater. Chem. Phys.*, 2014, **143**, 1164-1170.

278 J. C. Huang, P. P. Xu, D. X. Cao, X. B. Zhou, S. N. Yang, Y. J. Li, G. L. Wang, *J. Power Sources*, 2014, **246**, 371-376.

279 J. Y. Ji, L. L. Zhang, H. X. Ji, Y. Li, X. Zhao, X. Bai, X. B. Fan, F. B. Zhang, R. S. Ruoff, *ACS Nano*, 2013, **7**, 6237-6243.

280 Z. Tang, C. H. Tang, H. Gong, *Adv. Funct. Mater.*, 2012, **22**, 1272-1278.

281 X. Wang, J. Y. Liu, Y. Y. Wang, C. M. Zhao, W. T. Zheng, *Mater. Res. Bull.*, 2014, **52**, 89-95.

282 Y. G. Wang, D. D. Zhou, D. Zhao, M. Y. Hou, C. X. Wang, Y. Y. Xia, *J. Electrochem. Soc.*, 2013, **160**, 98-104.

283 J. Yan, Z. J. Fan, W. Sun, G. Q. Ning, T. Wei, Q. Zhang, R. F. Zhang, L. J. Zhi, F. Wei, *Adv. Funct. Mater.*, 2012, **22**, 2632-2641.

284 H. L. Wang, Y. Y. Liang, T. Mirfakhrai, Z. Chen, H. S. Casalongue, H. J. Dai, *Nano Res.*, 2011, **4**, 729-736.

285 J. W. Lang, L. B. Kong, M. Liu, Y. C. Luo, L. Kang, *J. Solid State Electrochem.*, 2010, **14**, 1533-1539.

286 J. H. Park, S. W. Kim, O. O. Park, J. M. Ko, *Appl. Phys. A*, 2006, **82**, 593-597.

287 X. X. Liu, C. Wang, Y. B. Dou, A. Zhou, T. Pan, J. B. Han, M. Wei, *J. Mater. Chem. A*, 2014, **2**, 1682-1685.

288 W. F. Zhang, C. Ma, J. H. Fang, J. P. Cheng, X. B. Zhang, S. R. Dong, L. Zhang, *RSC Adv.*, 2013, **3**, 2483-2490.

289 X. Wang, A. Sumboja, M. F. Lin, J. Yan, P. S. Lee, *Nanoscale*, 2012, **4**, 7266-7272.

290 H. L. Wang, Q. M. Gao, J. Hu, *J. Power Sources*, 2010, **195**, 3017-3024.

291 C. C. Hu, J. C. Chen, K. H. Chang, *J. Power Sources*, 2013, **221**, 128-133.

292 C. H. Lien, C. C. Hu, C. T. Hsu, D. S. H. Wong, *Electrochem. Commun.*, 2013, **34**, 323-326.

293 C. C. Hu, C. T. Hsu, K. H. Chang, H. Y. Hsu, *J. Power Sources*, 2013, **238**, 180-189.

294 Z. H. Sun, A. B. Yuan, *Chin. J. Chem. Eng.*, 2009, **17**, 150-155.

295 A. Shanmugavani, R. K. Selvan, *RSC Adv.*, 2014, **4**, 27022-27029.

296 I. Shakir, Z. Ali, J. Bae, J. Park, D. J. Kang, *RSC Adv.*,2014, **4**, 6324-6329.